Prediction of Turbulent Boundary Layers in Some Unusual Situations

By

ASHOK KUMAR SINGHAL

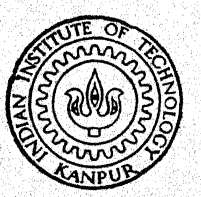

DEPARTMENT OF MECHANICAL ENGINEERING

INDIAN INSTITUTE OF TECHNOLOGY, KANPUR.

August 1970

401

PREDICTION OF TURBULENT BOUNDARY LAYERS IN SOME UNUSUAL SITUATIONS

A Thesis Submitted
In Partial Fulfilment of the Requirements
For the Degree of

MASTER OF TECHNOLOGY

401

by

ASHOK KUMAR SINGHAL

to the
Department of Mechanical Engineering,
INDIAN INSTITUTE OF TECHNOLOGY, KANPUR

August 1970

CERTIFICATE

This is to certify that this work has been carried out under my supervision and has not been submitted elsewhere for a degree.

S. V. Patankar

(S. V. Patankar)
Assistant Professor
Dept. of Mechanical Engg.
Indian Institute of Technology,
Kanpur

August, 1970

ACKNOWLEDGEMENT

I wish to express my deep sense of gratitude to Dr. S.V. Patankar for his guidance and encouragement throughout the course of this work. I owe him much for his sustained interest and for the lively discussions, for which he always had time. It was my privilege to have worked with him.

Ashok Kumar Singhal

ABSTRACT

Predictions of various flow and heat-transfer characteristics of a few practically-occurring turbulent boundary-layer flows have been made by using an implicit finite-difference technique, developed by Patankar and Spalding (1967). The problems considered are (a) wall jets on cylindrical surfaces, (b)axi-symmetrical boundary layers, (c) boundary-layer development on continuous moving surfaces, (d) free rotating disc, and (e) flow between a rotor and a stator. Each of these problems incorporates some unusual features.

The physical inputs include a form of Prandtl's mixing-length hypothesis and the supposition that the turbulent Prandtl number is uniform across the boundary layer. A simple modification to the mixing-length model is postulated for the swirling flows so that the effective viscosity remains a scalar quantity. The agreement between the predictions and the experimental data is, in general, very satisfactory. The novelty of the present work is that all the above-mentioned problems have been solved by the same calculation procedure and with the same set of hypotheses and constants which have been successfully used for more conventional situations.

CONTENTS

CHAPTER 1

INTRODUCTION

1.1 Background:

In the last few decades, the concepts of boundary-layer phenomena in general and turbulent boundary layer in particular have found application in a wide range of engineering fields. The physics of laminar flows is well understood. However, this is not so for turbulent flows. This means that the study of turbulent boundary layers must be a blend of theory and experimentation. The experiments yield much information of indispensable value, but it is neither possible nor advisable to conduct experiment for each new situation, one encounters in practice. What is needed is the capability of making predictions for the whole range of practically occurring boundary-layer flows with the use of as little empirical information as possible. Further, because of the increasing sophistications in technology, there is an ever-increasing need for more and more accurate predictions.

Recent progress in the development of prediction methods has been possible because of the increasing availability of faster and more economical digital computers. Even then until very recently, most of the procedures in common use were of the integral type, also known as 'approximate methods'. Inspite of their simplicity these methods may not prevail long because

different methods use empirical information in different forms. Further, their extention to new situations demands new empirical input. Therefore, it seems preferable to use finite-difference technique which requires empirical information at a more basic level and hence can treat a wider class of problems. So far, the finite difference method was thought of as very expensive in computing time, and hence was not in common use, although it was known that this method, in principle, can give accurate solutions. Patankar-Spalding (1967) developed a procedure that embodies devices which reduce the computing time to a very large extent and retain all the advantages of the finite-difference methods. This method is used in this thesis.

General remarks on the selection of problems and the calculation procedure:

The flow situations which have been considered here, are unusual in the sense that they are quite different from the conventional ones e.g. boundary layer development on a flat plate or on an aerofoil or in any other simple situation where velocity increases monotonically with cross stream distance. The problems have been so chosen that each incorporates one or more of the following special features:

(a) transverse curvature;

(b) maxima in the velocity profiles;

(c) moving solid surfaces;

(d) swirl velocity;

(e) confinement in a duct where pressure gradient is not known beforehand.

It is not implied here that these problems cannot be solved by other methods. In fact, some of them have already been tried by analytical and integral methods and in some cases, results do show good agreement with experiments. But unfortunately most of these methods are approximate ones and have been designed for particular problems. The approximate methods raise many questions to which the answers are absent or doubtful. Moreover, a practicing engineer would not like to acquaint himself with a host of solution procedures; rather he would prefer to master a single reliable method which can conveniently handle various problems of his interest. The calculation method which is used here, is reasonably accurate and meets most of the above-mentioned requirements.

1.2 The problems considered:

As mentioned earlier we shall consider only turbulent flow situations. The problems considered are:

1) Wall jets on cylindrical surfaces.
2) Axisymmetric boundary layers
3) Boundary-layer development on continuous moving surfaces.
4) Free rotating disc.
5) Flow between a rotor and a stator.

These problems will be briefly described below.

1) Wall jets on cylindrical surfaces:

There are numerous fluid-flow and heat-transfer processes which involve the interaction of a fluid jet with a solid surface.

A special feature of such flow configurations, commonly called wall jets, is that the velocity profiles exhibit a maxima. Plane and radial wall jets have already been studied quite extensively (Ref. 7). In recent years, consideration has been given to the cylindrical wall jet flows. A cylindrical wall jet is formed when a jet emerges from an annular slot and flows longitudinally and coaxially on a cylindrical rod (Fig. 1.1). Thus, it represents a configuration which possesses transverse surface curvature.

2) Axisymmetric boundary layers:

Here we shall be concerned with the turbulent boundary-layer flows over circular cylinders whose axes are alligned parallel to the free stream. In such flow situations the mean velocity profiles are found to be nonsimilar.

3) Boundary-layer development on continuous moving surfaces:

Flow on a continuous moving solid surface represents a new class of boundary layer problems, with solutions substantially different from those for boundary-layer flow on surfaces of finite length. A polymer sheet or filament extruded continuously from a die, or a long thread travelling between a feed roll and a wind-up roll, is an example of a continuous moving surface. Owing to the action of viscosity the motion of surface induces a motion in the adjacent fluid, and this region of flow penetrates deeper into the quiscent fluid environment with increasing distance from the slot. Thus the velocity boundary layer grows in the direction of

motion of the surface. This characteristic is just opposite to that for a semi-infinite flat plate moving through a quiescent environment wherein the boundary layer grows in the direction opposite to that in which the plate is moving. The essential features are illustrated schematically in Fig. 1.3.

4) Free rotating disc.:

The motion of fluid over a rotating disc, poses problems of widespread practical interest in connection with turbines, pumps and other rotating fluid machines. The idealisation of the portion of the rotating element between the shaft and blading for an axial machine as a plane circular disc, has been frequently found to be useful. A simple sketch showing radial and tangential velocity profiles is shown in Fig. 1.4.

5) Flow between a rotor and a stator:

This problem illustrates the effects of a super imposed radial outflow upon the motion of the fluid between a rotating and a stationary plane disc. This is an idealisation of the situation found in advanced turbomachinery in which cooling of the roter-faces is necessary. In modern gas turbine practice, as maximum gas temperature continually increases, a radially outward flow of cooling air is forced from near the axis between the rotating and stationary members to maintain the material temperature at an acceptable level. Necessary details of the configuration are shown in Fig. 1.5. It can be seen in

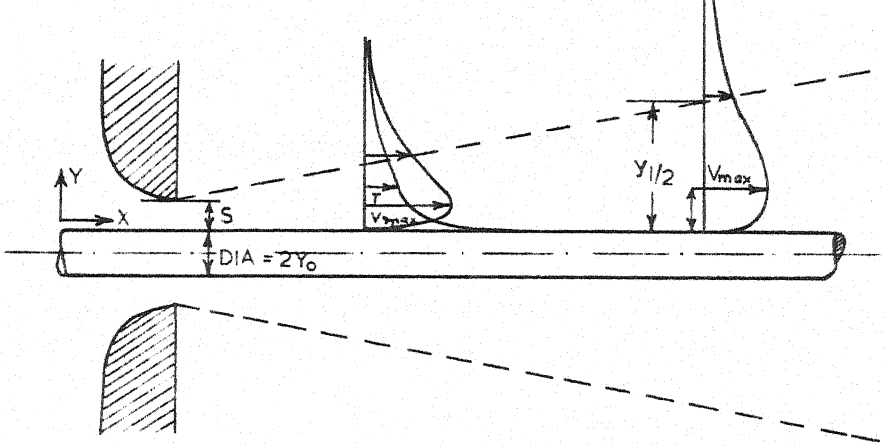

FIG. 1.1 THE CYLINDRICAL WALL JET

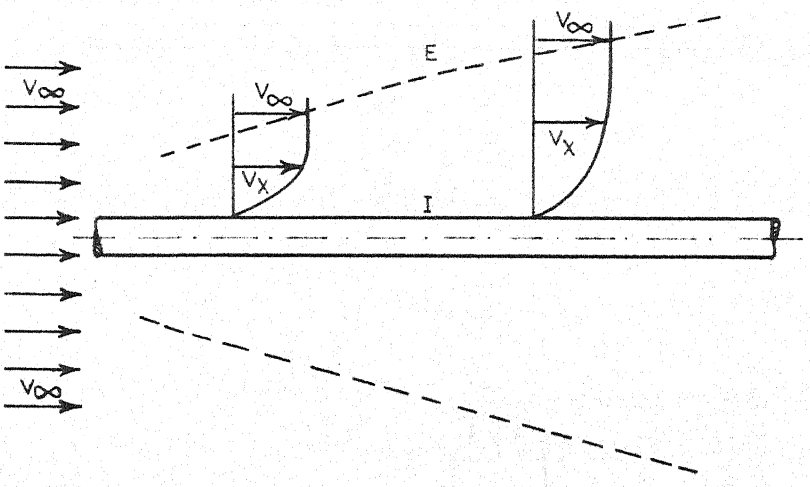

FIG. 1.2 AXISYMMETRICAL BOUNDARY LAYER

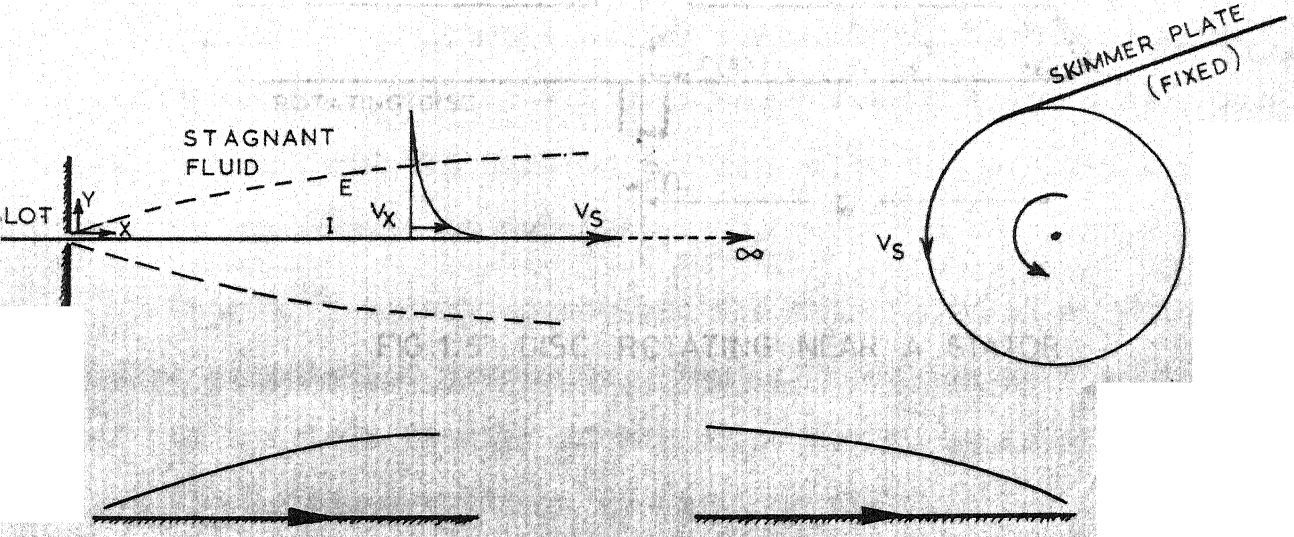

(a) CONTINUOUS MOVING SURFACE (b) SEMI-INFINITE PLATE

FIG. 1.3 BOUNDARY LAYER DEVELOPMENT ON A CONTINUOUS MOVING SURFACE

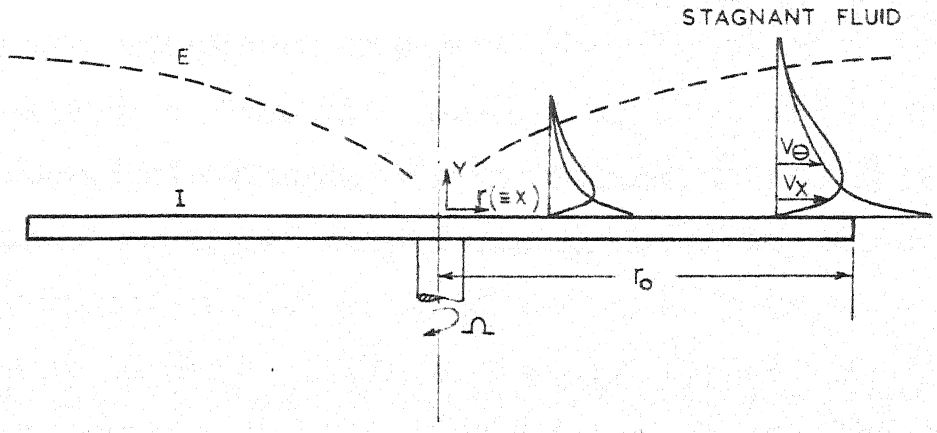

FIG.1.4 FREE ROTATING DISC

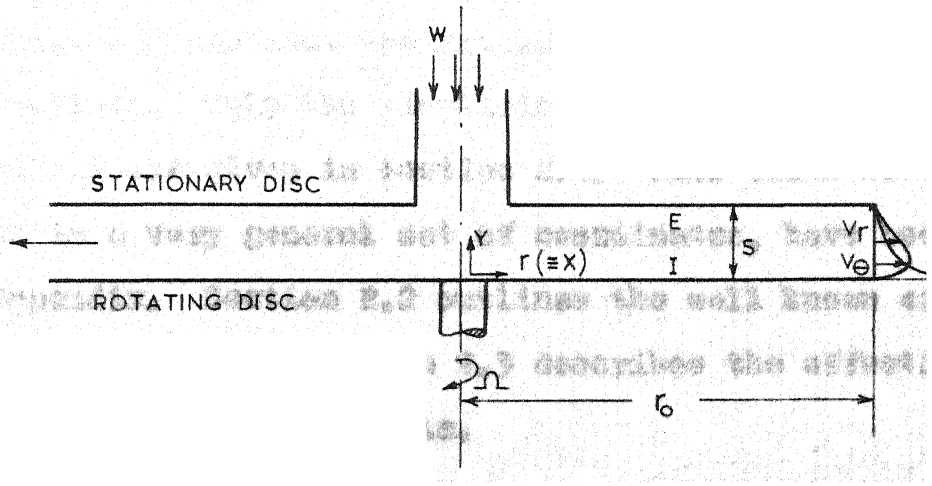

FIG.1.5 DISC ROTATING NEAR A STATOR

Chapter 4 that how profoundly such a flow is influenced by the relative diameter and spacing of the stationary coaxial member.

1.3 Outline of the thesis:

The aim of the present work is to illustrate the versatility of the calculation procedure (Ref. 7) and to assess the satisfactoriness of Prandtl's mixing-length hypothesis for the above mentioned situations. The description of the conventional conservation laws and of the calculation procedure has been made as brief as possible; the pride of the place is given to the modifications to mixing-length hypothesis for swirling flows and also to the solution procedure for confined flows. The general arrangement of the remaining material is as follows.

Chapter 2 includes the mathematical and physical aspects of the problems. Only the simplified forms of the basic governing equations are given in Section 2.1. Full forms of these equations in a very general set of coordinates, have been given in the Appendix. Section 2.2 outlines the well known effective-exchange laws, and the Section 2.3 describes the effective-viscosity hypothesis in details.

Chapter 3 briefly describes the main features of Patankar-Spalding calculation procedure. The last section of this chapter gives the complete details of the procedure to be adopted to calculate the pressure gradient in confined flows.

Discussion of the results of the computations and the comparison of the same with the available experimental data has been presented in Chapter 4. To make the comparisons more meaningful, a brief account of experimental studies of various authors is made for each problem.

Chapter 5 contains the concluding remarks and few suggestions for the future work.

CHAPTER 2

MATHEMATICAL AND PHYSICAL FOUNDATIONS

2.1 The conservation equations

The conservation laws in question represent the conservation of

(i) mass (the continuity equation);

(ii) momentum in the x-direction ;

(iii) momentum in the θ-direction;

(iv) enthalpy (the First Law of Thermodynamics).

From the description of Section 1.2, it is obvious that the boundary-layer approximations are valid for all the flow situations to be considered herein. In the Appendix we have given the boundary-layer equations in a very general axi-symmetric coordinate system. The simplified forms of these basic equations for our flow geometries are as follows:

Continuity:

$$\frac{\partial}{\partial x}(\rho V_x r) + \frac{\partial}{\partial y}(\rho V_y r) = 0 \qquad (2.1\text{-}1)$$

Momentum:

$$\rho V_x \frac{\partial V_x}{\partial x} + \rho V_y \frac{\partial V_x}{\partial y} = \frac{1}{r}\frac{\partial}{\partial y}(\tau_x r) - \frac{dp}{dx} \qquad (2.1\text{-}2)$$

Enthalpy:

$$\rho V_x \frac{\partial h}{\partial x} + \rho V_y \frac{\partial h}{\partial y} = -\frac{1}{r}\frac{\partial}{\partial y}(qr) \qquad (2.1\text{-}3)$$

For the rotating disc problems, continuity equation remains unaltered and the other two equations to be solved are:

Conservation of momentum in the radial ($r \equiv x$) direction:

$$\rho\left(V_x \frac{\partial V_x}{\partial x} + V_y \frac{\partial V_x}{\partial y} - \frac{V_\theta^2}{r}\right) = \frac{\partial}{\partial y}(\tau_x) - \frac{dp}{dx} \qquad (2.1\text{-}4)$$

Conservation of momentum in the tangential (θ) direction:

$$\rho\left(V_x \frac{\partial V_\theta}{\partial x} + V_y \frac{\partial V_\theta}{\partial y} + \frac{V_\theta V_x}{r}\right) = \frac{\partial \tau_\theta}{\partial y} \qquad (2.1\text{-}5)$$

where the symbols have the significance given in the nomenclature. The distance x is measured in the direction of the flow, and y is measured perpendicular to it from a specified boundary of the flow called the I (internal) boundary. The radius r is measured from the axis of symmetry. It is very interesting and important to note that in the first two problems r varies in the y direction, in the last two problems it coincides with the x coordinate and in the third problem r has no significance.

2.2 Exchange laws:

The quantities like shear stress and heat flux are best represented by the following exchange laws:

$$\tau_x = \mu_{eff} \frac{\partial V_x}{\partial y} \qquad (2.2\text{-}1)$$

$$\tau_\theta = \mu_{eff} \frac{\partial V_\theta}{\partial y} \qquad (2.2\text{-}2)$$

$$q = -\left(\frac{\mu_{eff}}{\sigma_{eff}}\right)\left(\frac{\partial h}{\partial y}\right) \qquad (2.2\text{-}3)$$

where μ_{eff} and σ_{eff} are the effective viscosity and effective Prandtl number respectively. In the following section we discuss the central problem of turbulent boundary layers - how to relate the effective-exchange coefficients to the local fluid state.

2.3 Effective-viscosity hypothesis:

We shall use the Prandtl's mixing-length hypothesis that characterises the local state of turbulence by a local mean-velocity gradient and a local length scale. Since the considered flow situations involve presence of a wall, two sets of hypothesis will therefore be used one for the fully-turbulent region and the other for the wall-near region.

Fully-turbulent region:

For this region the mixing-length hypothesis can be expressed as

$$\mu_{eff} = \rho l^2 \left| \frac{\partial V_x}{\partial y} \right| \qquad (2.3\text{-}1)$$

where l is the mixing length. We shall use the following variation of the mixing length.

$$\begin{aligned} 0 < y \leq \frac{\lambda y_1}{K} \quad &: \quad l = Ky \\ \frac{\lambda y_1}{K} < y \quad &: \quad l = \lambda y_1 \end{aligned} \qquad (2.3\text{-}2)$$

This variation has been found to agree with large amount of

experimental data. K and λ are constants, y is the distance from the wall, and y_1 is a characteristic thickness of the layer. The values used are:

$$K = 0.435 , \qquad \lambda = 0.09$$

and y_1 is taken equal to the boundary layer thickness δ: defined as the distance, from the wall, of a point (near the free boundary) at which the velocity differs from the free stream velocity by one percent of the maximum velocity-difference across the layer. In the confined flow where both the boundaries are walls, it is assumed as if seperate boundary layer grows on each wall.

Wall-near region:

The above-mentioned formulae neglect the laminar contribution to the effective viscosity. This is satisfactory for most part of the layer, because the turbulent contribution is much greater than the laminar one. However, in the vicinity of a wall the magnitude of the turbulent viscosity diminishes and becomes comparable to the laminar viscosity. Thus, a more detailed hypothesis describing the respective roles of turbulent and molecular viscosities should be used for these regions.

We shall use the Van Driest's hypothesis (1956). With a modification suggested in Ref. 5., it takes the following form:

$$\mu_{eff} = \mu + \rho K^2 y^2 \left[1-\exp\left\{-y\sqrt{\tau\rho}/(A\mu)\right\}\right]^2 \left| \frac{\partial V_x}{\partial y} \right| \qquad (2.3\text{-}3)$$

This hypothesis implies that μ_{eff} is composed of the laminar viscosity μ and the turbulent viscosity $\rho K^2 y^2 \left| \frac{\partial V_x}{\partial y} \right|$, which

gets damped near the wall in an exponential fashion.

Fig. 2.1 shows the mixing-length distribution for the whole layer. Two points should be emphasized here: First is that we are using exactly the same set of constants which have been successfully used for a large number of conventional situations such as boundary layers on smooth walls with various pressure gradients (Ref. 5) and many other situations as reported in Ref. 6, 7, 12 and 14. Secondly we are not making any change from problem to problem.

Modifications to the effective-viscosity formulae for swirling flows:

Eqn. (2.3-1), as such, cannot be used for swirling flows, because for every point there are two velocity components and hence two different velocity gradients. Since there are no hypotheses available for such flow situations, expressions similar to Eqn. (2.3-1) could be used with a modified value of velocity gradient. It seems plausible that μ_{eff} should be a function of both the gradients. A simple choice will be to use some sort of mean of the two gradients. We have made computations using both arithmetic-mean and the root-mean-square (RMS) value of the gradients. The proposed expressions for μ_{eff} are:

$$\mu_{eff} = \rho l^2 \frac{1}{I} \sum_i \left| \frac{\partial V_i}{\partial y} \right| \qquad (2.3\text{-}4)$$

$$\mu_{eff} = \rho l^2 \sqrt{\frac{1}{I} \sum_i \left(\frac{\partial V_i}{\partial y} \right)^2} \qquad (2.3\text{-}5)$$

here i takes the value 1 or 2 depending upon whether the flow is without swirl or with swirl. V_1 and V_2 will have the same meaning as V_x and V_θ respectively.

It must be admitted here that there is no physical justification for using either a mean or a RMS value, and one can probably find many better ways. However, the predictions obtained with these modifications are in reasonable agreement with the experiments, as shown in Sections 4.5 and 4.6. From the present problems there is very little to choose between the two suggestions, yet the RMS value seems to be slightly better.

Some authors (Ref. 1) have used two different viscosities determined by respective velocity gradients in the two directions. However, their results are not very encouraging. Otherwise also, it can be proved by rigorous analysis that the effective viscosity has to be either a scalar quantity or a fourth-order tensor.

2.4 Effective Prandtl number:

For the prediction of heat transfer characteristics, the effective Prandtl number is taken as uniform across the layer and is put equal to 0.9. Near a wall, the extra resistance of the laminar sublayer is taken into account by use of Van Driest's hypothesis:

$$\frac{\mu_{eff}}{\sigma_{eff}} = \frac{\mu}{\sigma} + \frac{\rho \kappa^2 y^2}{\sigma_t} \left[1-\exp\left\{-y\sqrt{\tau\rho/(\mu A^+)}\right\}\right]^2 \left|\frac{\partial V_x}{\partial y}\right| \quad (2.4\text{-}1)$$

where σ and σ_t are respectively the laminar and turbulent Prandtl numbers.

With this much of mathematical and physical background, we proceed to the solution-procedure.

CHAPTER 3

THE SOLUTION PROCEDURE

As mentioned earlier, we shall use Patankar-Spalding solution procedure which has been exhaustively described in Ref. 7. For the convenience of the reader, the salient features of the method are briefly mentioned in the following sections. Section 3.6 is particularly important as it contains information not given in Ref. 7. It deals with the calculation of pressure gradient in confined flows.

3.1 Self-adjusting grid:

The method employs a self adjusting grid which always conforms to the thickness of the physical boundary layer. Thus, attention is concentrated on the essentials only, which in turn leads to a great economy in computation time. It is achieved by using a non-dimensional stream function as the cross stream variable and an appropriate formula for the entrainment rate at the free boundary. The region of interest is supposed to lie between two boundaries - the internal one (I) and the external one (E). Some of the important terms are defined below.

Stream function :

$$x = \text{fixed}; \quad d\psi = \rho V_x \, r \, dy \qquad (3.1\text{-}1)$$

Non-dimensional stream function :

$$\omega = \frac{\psi - \psi_I}{\psi_E - \psi_I} \qquad (3.2\text{-}2)$$

It follows that ω equals zero at I boundary and unity at E. From the definition of stream function we also have,

$$\frac{d\psi_I}{dx} = - r_I \dot{m}_I'' \qquad (3.1\text{-}3)$$

and

$$\frac{d\psi_E}{dx} = - r_E \dot{m}_E'' \qquad (3.1\text{-}4)$$

where $\dot{m}_I''$ and $\dot{m}_E''$ are the rates of mass transfer across the I and E surfaces. These relations will be used in determining the entrainment rates at the free boundaries.

3.2 Equations in $x \sim \omega$ coordinates:

The equations of conservation of momentum, enthalpy etc. are all transformed into $x \sim \omega$ system. Thus we have,

Conservation of momentum in the x-direction:

$$\frac{\partial V_x}{\partial x} + \frac{\{r_I \dot{m}_I'' + \omega(r_E \dot{m}_E'' - r_I \dot{m}_I'')\}}{(\psi_E - \psi_I)} \frac{\partial V_x}{\partial \omega} =$$

$$\frac{\partial}{\partial \omega} \left\{ \frac{r^2 \; V_{x\,eff}}{(\psi_E - \psi_I)^2} \frac{\partial V_x}{\partial \omega} \right\} - \frac{1}{\rho V_x} \left(\frac{dp}{dx} - \frac{V_\theta^2}{r} \right) \qquad (3.2\text{-}1)$$

Conservation of momentum in the θ direction:

$$\frac{\partial}{\partial x}(r V_\theta) + \frac{r_I \dot{m}_I'' + \omega(r_E \dot{m}_E'' - r_I \dot{m}_I'')}{(\psi_E - \psi_I)} \frac{\partial(r V_\theta)}{\partial \omega} =$$

$$\frac{\partial}{\partial \omega}\left\{\frac{r^2 \rho V_x \mu_{eff}}{(\psi_E - \psi_I)^2} \frac{\partial(r V_\theta)}{\partial \omega}\right\} \qquad (3.2\text{-}2)$$

Conservation of enthalpy:

$$\frac{\partial h}{\partial x} + \frac{r_I \dot{m}_I'' + \omega(r_E \dot{m}_E'' - r_I \dot{m}_I'')}{(\psi_E - \psi_I)} \frac{\partial h}{\partial \omega} =$$

$$\frac{\partial}{\partial \omega}\left\{\frac{r^2 \rho V_x \mu_{eff}}{(\psi_E - \psi_I)^2 \sigma_{eff}} \frac{\partial h}{\partial \omega}\right\} \qquad (3.2\text{-}3)$$

These equations possess the common form:

$$\frac{\partial \phi}{\partial x} + (a + b\omega)\frac{\partial \phi}{\partial \omega} = \frac{\partial}{\partial \omega}\left(c \frac{\partial \phi}{\partial \omega}\right) + d \qquad (3.2\text{-}4)$$

where $a = r_I \dot{m}_I'' / (\psi_E - \psi_I)$ (3.2-5)

$$b = (r_E \dot{m}_E'' - r_I \dot{m}_I'') / (\psi_E - \psi_I) \qquad (3.2\text{-}6)$$

$$c = r^2 \rho V_x \mu_{eff} / (\psi_E - \psi_I)^2 \sigma_{eff}$$

Here ϕ stands for the dependent variable and the last term d, which does not contain $\partial\phi/\partial\omega$ is known as the source term. It expresses the influence of the 'sources' of the entity ϕ. For the present cases, particular expressions for d are given in the following table.

Table: Expressions for d

Dependent variable	Expression for d
V_x	$-\frac{1}{\rho V_x}\frac{dp}{dx}$
V_x (for swirling flows)	$-\frac{1}{\rho V_x}\left(\frac{dp}{dx}-\frac{V_\theta^2}{r}\right)$
$r V_\theta$	0
h	0

It is important to note that the dependent variable of Eqn. (3.2-2) is rV_θ. It has some definite advantages, for example, the source term is minimised if rV_θ rather than V_θ is used as the dependent variable; this promotes the stability of the numerical procedure.

3.3 Entrainment rates:

When a boundary is free, an auxiliary relation to determine the mass transfer rate across it, commonly known as the entrainment rate, assumes vital importance in controlling the physical width of the grid. A straight-forward way of obtaining the following expression for entrainment rates has been outlined in Ref. 7.

$$\dot{m}_e'' = \lim_{\omega \to \omega_e} \left[\frac{\frac{\partial}{\partial \omega}\left(\frac{r^2 \rho u \mu_{eff}}{(\psi_E - \psi_I)}\frac{\partial u}{\partial \omega}\right)}{\partial u / \partial \omega} \right] \qquad (3.3\text{-}1)$$

it can also be written as:

$$r_G \dot{m}_G'' = \lim_{y \to y_G} \left[\frac{\frac{\partial}{\partial y}\left\{ r\mu_{eff} \frac{\partial u}{\partial y} \right\}}{\partial u/\partial y} \right] \qquad (3.3\text{-}2)$$

where subscript G stands for the free boundary. Eqn. (3.3-2) is transformed into a finite-difference form which can be incorporated in the computer program.

3.4 Wall functions:

It is well known that both the dependent variable and the effective exchange coefficients vary steeply in the wall-near region. As a consequence, substantial computation time may be required for the good accuracy of this narrow, but importan region. In the present method considerable economy is achieved, by use of Couette-flow solutions which are obtained on the following lines.

Near a wall, the velocity V_x is small and therefore, the x-wise convection is locally negligible. Thus, there exists a one dimensional boundary layer near the wall; this is also known as the Couette flow. The flow problem in this region is reduced to the solution of an ordinary rather than partial differential equation. In Ref. 7, integrations of the resulting one-dimensional equations have been performed by use of Van Driest hypothesis (Eqn. (2.3-3)), and the results have been finally transformed into convenient algebraic forms. These formulae are called as

'wall functions' or as 'wall-flux relationships'; they relate the flux at the wall, of momentum, matter or enthalpy to the values of velocity, concentration, temperature etc.

We shall now mention below only those formulae which are used in the present work. First we define the main dimensionless quantities used in these formulae.

$$R = \frac{\rho V_x y}{\mu}, \qquad P = \frac{y}{\rho V_x^2}\frac{dp}{dx}$$

$$s = \frac{\tau}{\rho V_x^2}, \qquad S = \frac{q}{\rho V_x (h_s - h)} \tag{3.4-1}$$

For convenience these are further transformed as:

$$R_* = RK^2, \qquad P_* = P/K^2$$

$$s_* = s/K^2, \qquad S_* = S/K^2 \tag{3.4-2}$$

The formulae used are:

(1) The drag law (when $P_* = 0$):

$$s_{*,0} = K_0^{-1} - 0.1561\, R_*^{-0.45} + 0.08723\, R_*^{-0.3} + 0.03713 R_*^{-0.18} \tag{3.4-3}$$

(2) The drag law (when $P_* \neq 0$):

$$\frac{s_*}{s_{*,0}} = \left[1 - \frac{4P_*R_*}{(12.8^{2.5} + R_*^{2.5})^{0.4}} \right]^{1.6} \tag{3.4-4}$$

(3) The flux law (For $F_* = 0$)

$$S_{*,0} = \frac{s_{*,0}}{1 + P_*(s_{*,0})^{1/2}} \qquad (3.4\text{-}5)$$

where $P_* = 3.68\,(\sigma/\sigma_t)^{-0.25}\,(\frac{\sigma}{\sigma_t} - 1)$.

Modification for moving surfaces:

When a surface is moving in the longitudinal direction, as is the case in Problem 3, the above-mentioned formulae can be used if the velocity V_x is replaced by the relative velocity $(V_s - V_x)$. Similarly for the flows on rotating surfaces, a relative tangential velocity $(V_0 - V_\theta)$ should be used in place of V_θ. However, for the swirling flows (surface may be rotating or may not be) we need some further adjustments.

Modification for swirling flows:

In swirling flows it is customary to specify wall shear stress in radial and tangential directions seperately. It is however for the sake of convenience or convention only. In reality a fluid particle near a wall has a spiral motion. Realising this we can use the same wall functions to know the values of shear stress in the actual direction of motion. Procedure is as follows:

First we find out the direction and magnitude of the resultant velocity from the known values of V_x and V_θ. Then instead of V_x, the resultant velocity is used in Eqn. (3.4-1)

to determine the non-dimensional quantities like R, s etc. Using Eqn. (3.4-2) and Eqn. (3.4-3) we get shear stress in the direction of resultant velocity. Finally it is resolved into two components to get the shear stresses in the desired directions.

3.5 Formulation and solution of finite-difference equations:

In the present method, a finite-difference equation is obtained by expressing each term in the parent partial differential equation as an integrated average over a small control volume (Fig. 3.1). Or in other words, for each grid node we formulate a micro-integral equation. When calculating the integrals, it is presumed that the main variables possess profiles which are made up of chains with straight-line links; and when transport in the cross-stream direction is considered, only the downstream values of the variables are used. Thus the method is an implicit one. It should suffice here to mention that implicit methods are comparatively stable and allow a larger forward step.

A difference equation, obtained as explained above, can be reduced to the form:

$$\phi_D = A\,\phi_{D++} + B\,\phi_{D--} + C \qquad (3.5\text{-}1)$$

where A, B and C are known in terms of the ϕ values of the upstream station. Thus at $x = x_D$, we obtain one difference equation for each grid node, and finally we possess a set of linear algebraic equations. These equations are solved by a simple successive-substitution method.

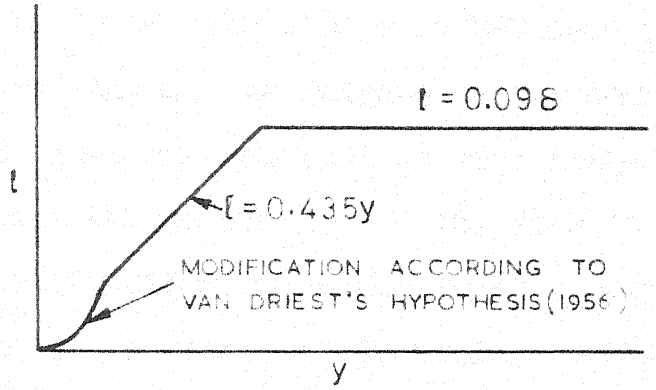

FIG. 2.1 MIXING-LENGTH DISTRIBUTION (USED FOR ALL THE PROBLEMS)

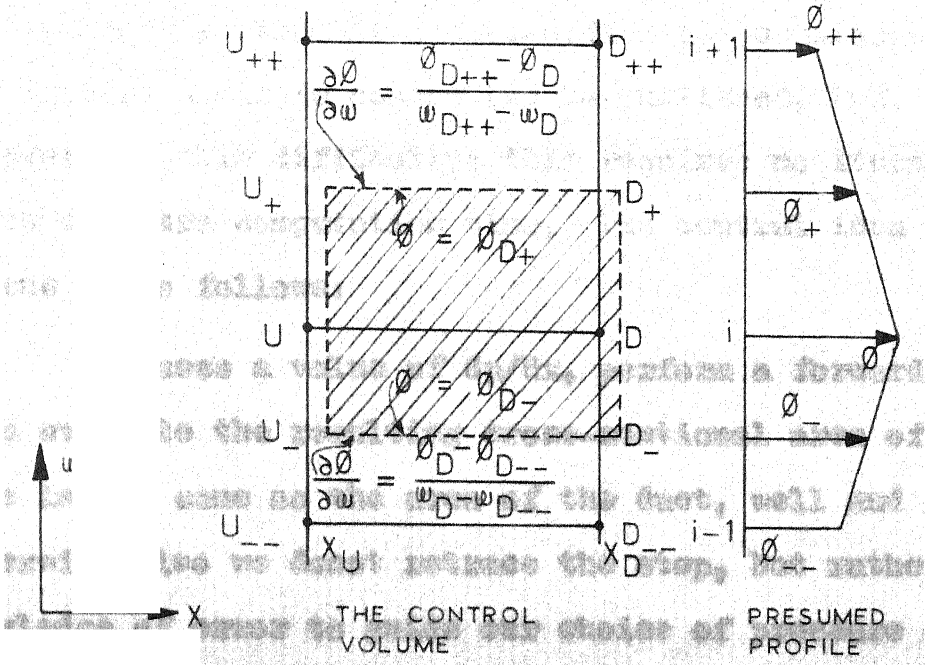

FIG. 3.1 A SMALL PART OF THE GRID, SHOWING A TYPICAL CONTROL VOLUME (SHADED) FOR WHICH THE MICRO-INTEGRAL EQUATION IS FORMULATED, AND ILLUSTRATING THE LINEAR-PROFILE ASSUMPTION.

It should be noted that when ϕ stands for V_x, its difference equation will not be reduced to the same form as (3.5-1) unless the pressure gradient is also known in addition to the upstream values of V_x. If the flow is external there is no difficulty about it, however, it is not so for the confined flows and a separate discussion is warranted.

3.6 Treatment of Confined Flows:

When the flow is confined e.g. in a duct (for the sake of generality), the pressure gradient dp/dx is not known prior to the solution of the boundary-layer equations. Therefore, it becomes an additional unknown and should be calculated simultaneously with the finite-difference equations for boundary layer. A simple scheme (to be published, Ref. 8) is used to overcome this difficulty; this requires no iterations and hence no extra computation time. The central idea of the scheme is as follows:

We guess a value of dp/dx, perform a forward step and then evaluate the resulting cross-sectional area of flow. If this is the same as the area of the duct, well and good; otherwise also we donot retrace the step, but rather use this knowledge of error to guide our choice of pressure gradient for the next forward step. Since we do not know how the profiles of velocity and density (in the case of compressible flow) will change during the course of a forward step, it is difficult to calculate the pressure gradient exactly. However, if we neglect these changes, we can derive a formula for pressure gradient directly from the equation of continuity and momentum.

If we further make an assumption of one-dimensional flow, the equations will be as follows:

Continuity:

$$\frac{dA}{A} = \frac{d\dot{m}}{\dot{m}} - \frac{d\bar{u}}{\bar{u}} - \frac{d\bar{\rho}}{\bar{\rho}} \qquad (3.6\text{-}1)$$

Momentum:

$$A dp + F' dx + \bar{u}\, d\dot{m} + \dot{m}\, d\bar{u} = 0 \qquad (3.6\text{-}2)$$

where A = cross-sectional area of the duct

$\dot{m}$ = mass flow rate of fluid

$\bar{\rho}$ = reference value of density

$\bar{u}$ = a particular average of velocity

$$= \int_{\text{duct}} r\rho u^2\, dy \Big/ \int_{\text{duct}} r\rho u\, dy$$

F' = retarding force per unit duct length, exterted by the walls and body forces.

Combination of Equations (3.5-1) and (3.5-2) leads to a general formula for dp/dx.

$$\frac{dp}{dx} = -\frac{F'}{A} - \frac{2\bar{u}}{A}\frac{d\dot{m}}{dx} + \frac{\dot{m}\bar{u}}{A}\left(\frac{1}{A}\frac{dA}{dx} + \frac{1}{\bar{\rho}}\frac{d\bar{\rho}}{dx}\right) \qquad (3.6\text{-}3)$$

The force F' is often provided by the shear stresses at the walls.

$$\frac{F'}{A} = \frac{2\pi(\tau_R r_R - \tau_I r_I)}{A} \qquad (3.6\text{-}4)$$

If the flow is incompressible and walls are impervious, the formula for dp/dx reduces to the following form.

$$\frac{dp}{dx} = \frac{\dot{m}\dot{m}}{A^2}\frac{dA}{dx} - \frac{F'}{A} \qquad (3.6\text{-}5)$$

Here the area-increment term is the most important one. It requires us to distinguish between the cross-sectional area of the <u>duct</u> A_d and that of <u>flow</u> A_f. Let the additional subscripts D and U denote downstream and upstream conditions, then the term dA/dx can be calculated from

$$\frac{dA}{dx} = \frac{A_{d,D} - A_{f,U}}{x_D - x_U} \qquad (3.6\text{-}6)$$

Here we have chosen the duct area for the down stream position, because that is the area we want the flow to acquire at the end of the step, and the flow area for the upstream position, because this represents the condition from which the flow actually starts. It is helpful to consider the numerator of Eqn.(3.6-6) as

$$A_{d,D} - A_{f,U} = (A_{d,D} - A_{d,U}) + (A_{d,U} - A_{f,U}) \qquad (3.6\text{-}7)$$

here the first term comprises the area increment which results from the change in duct-geometry, and the second represents the error i.e. the discrepancy between the flow area and the duct area.

The beauty of the above formulation is that it will always provide a pressure gradient that will tend to make the area-discrepancy diminish; the bigger the error, the bigger this tendency will be. If ever the difference between the duct and flow areas exceeds a pre-specified limit, it can be

remedied by reducing the forward step. Similarly if $(A_{d,U} - A_{f,U})$ is uneconomically small, the step-size can be enlarged.

The above scheme is very easily incorporated in the computer program and thus it enables us to treat the confined flows more or less in the same fashion as un-confined flows. Satisfactoriness of the scheme can be judged from the results presented in Section 4.6 (Fig. 4.15 and 4.16). Now in the following Chapter we compare our predictions with the available experimental data for the respective problems.

CHAPTER 4

COMPARISON OF PREDICTIONS WITH EXPERIMENTAL DATA

Before discussing the results for each problem separately, we should mention important computational details, which are more or less the same for all the problems.

4.1 Details of Computations:

The number of grid lines across the layer was taken as 20. In general, grid was made comparatively finer in the region near to a wall or to a point of the maximum velocity. The forward step size in the x-direction varied from 1/10th to 1/2 of the boundary-layer thickness. Appropriate power-law profiles or the experimental profiles, if available, were used as the initial conditions of the dependent variables; however the selection of initial profiles was not crucial. The fluid properties were regarded as uniform.

All the computations were performed on the IBM 7044 computer at IIT Kanpur. The computation time for each problem was quite modest. Some of the computations were repeated with a finer grid to ensure x that no numerical approximation was involved.

4.2 Cylindrical Wall Jet:

Starr and Sparrow (1967) were first to report the useful experimental information concerning the stream-wise development of a cylindrical wall-jet flow. They used an 1/2" diameter

rod with a convergent nozzle having exit dia equal to 0.667", and conducted experiments for two Reynolds numbers. Thus they used only one geometry, and the curvature parameter C($\equiv$ rod diameter/slot height) was equal to 5.9).

Recently, Manian, Mc Donald and Bennt (1969) have reported a more extensive study which covers a large range of curvature parameter c and slot-Reynold numbers. Their experiments also included the heat transfer-measurements. They used 1/4" and 1/8" dia. stainless-steel rods. At the nozzle exit uniform flow was maintained at room temperature. Measurements were taken for the constant heat flux at the surface of the cylinders.

The Flow Characteristics:

The streamwise development of a wall-jet flow is best characterized by the grow of the jet thickness $y_{1/2}$ and the decay of the maximum velocity $V_{max.}$. Fig. 4.1 shows that both of these predicted characteristics are in excellent agreement with the experimental data of Ref. 13. Similar agreement was found for the other Reynolds number (50,000) also (not shown in the figure).

Predictions of jet spread and velocity decay were also made for each of the curvature parameter values used by Manian et al (1969). Comparisons with the experimental data are shown in Fig. 4.2 and 4.3; and the agreement is seen to be very good except for the smaller values of c, where the departure could possibly be attributed to high turbulence in

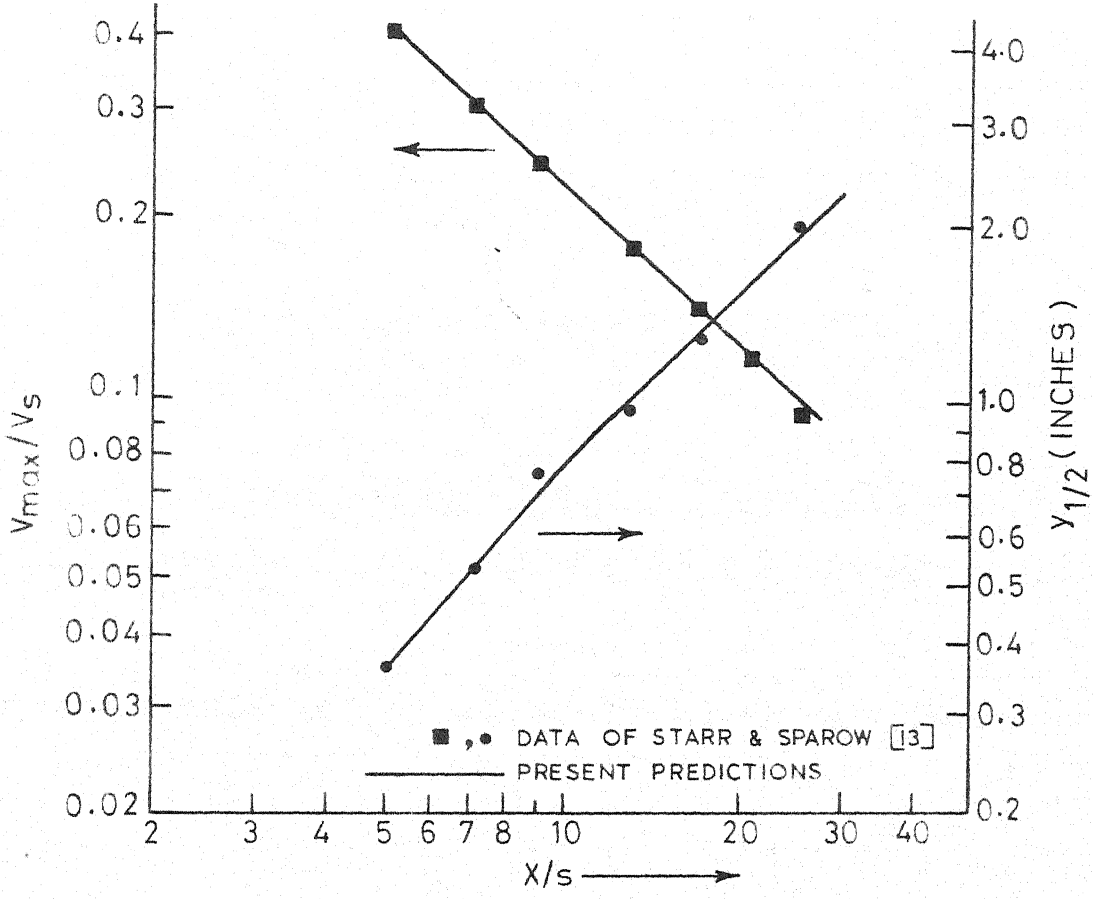

FIG. 4.1 JET SPREAD AND VELOCITY DECAY ($Re_s = 27000$)

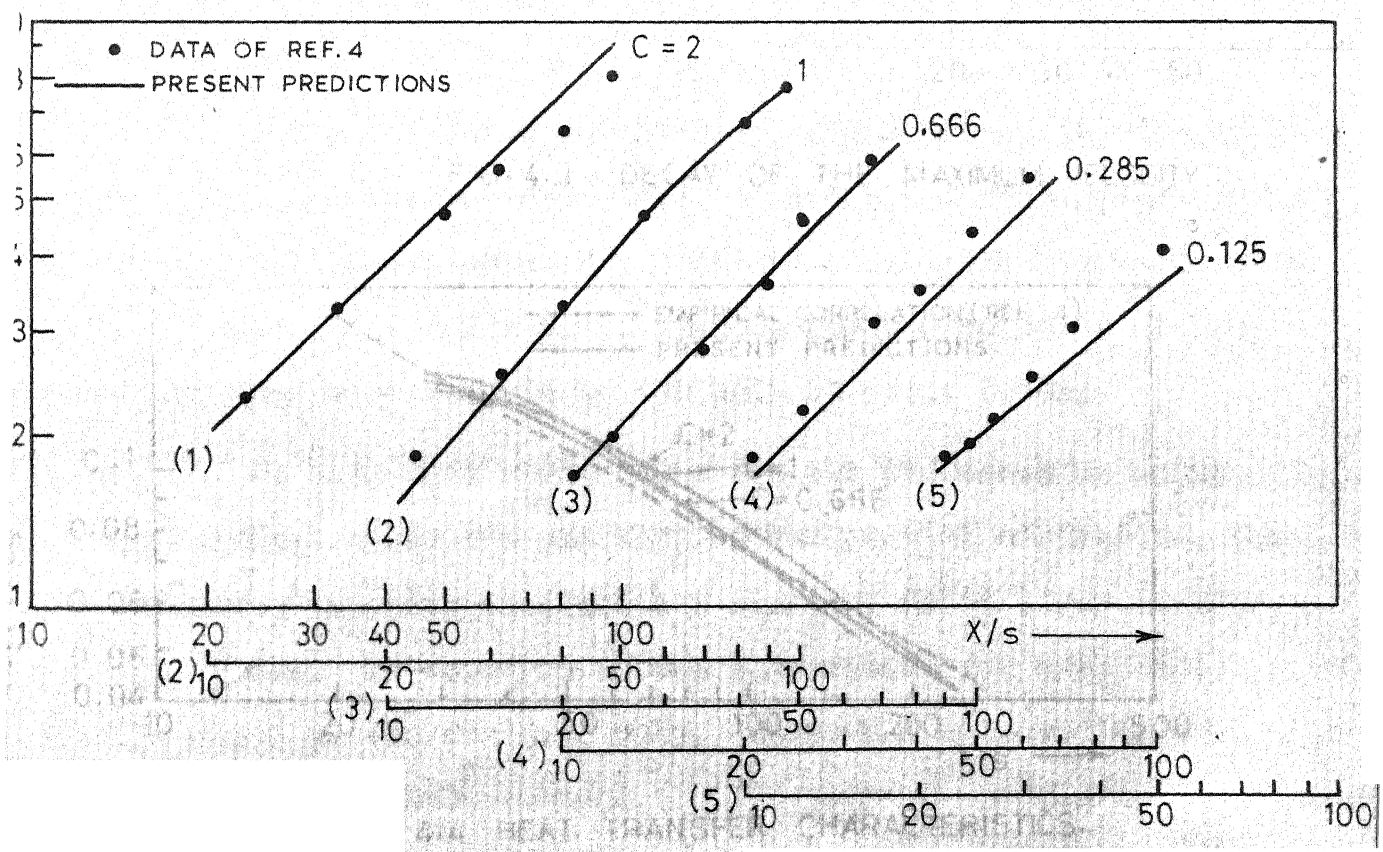

FIG. 4.2 SPREAD OF WALL JET

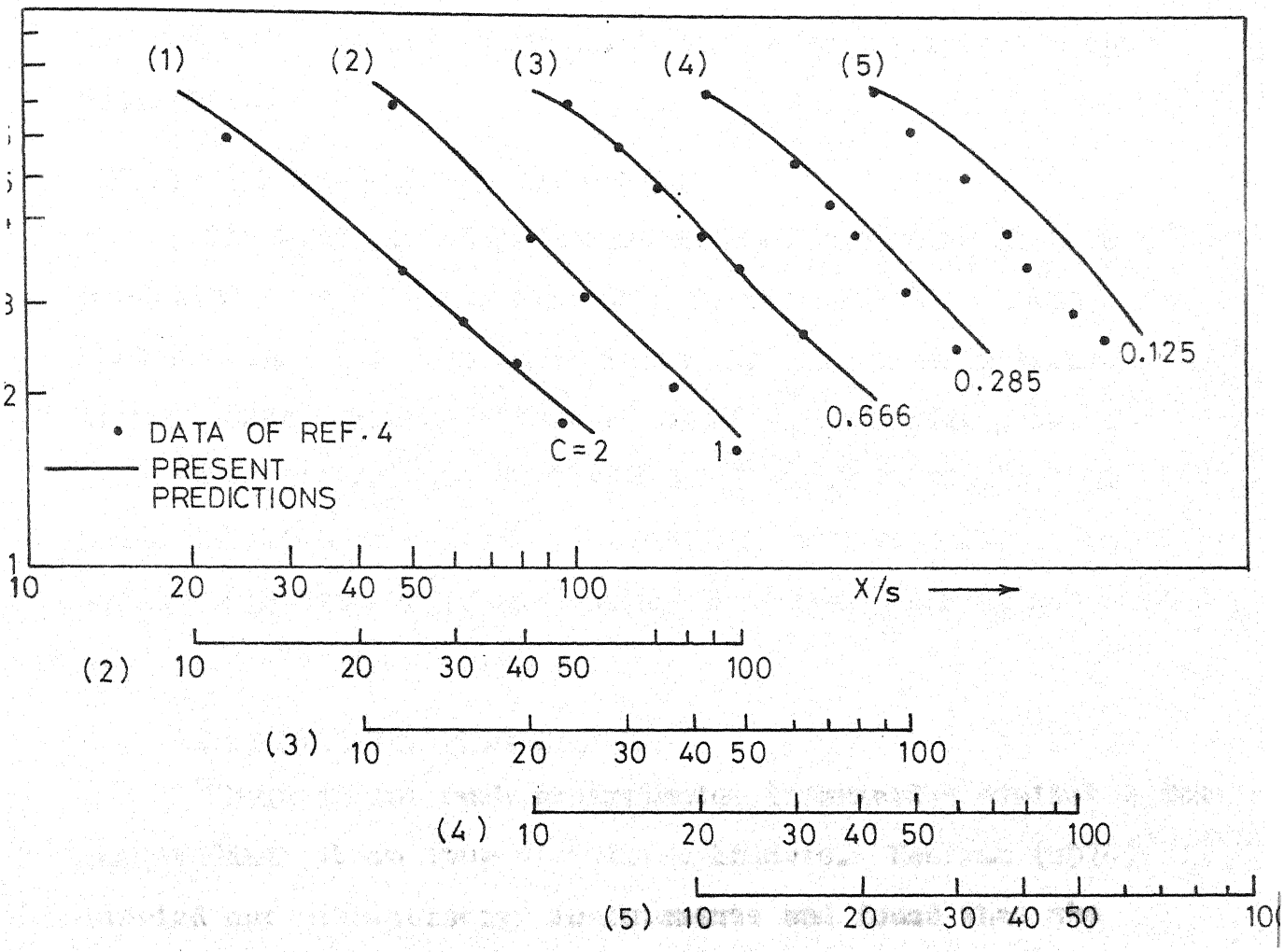

FIG. 4.3 DECAY OF THE MAXIMUM VELOCITY

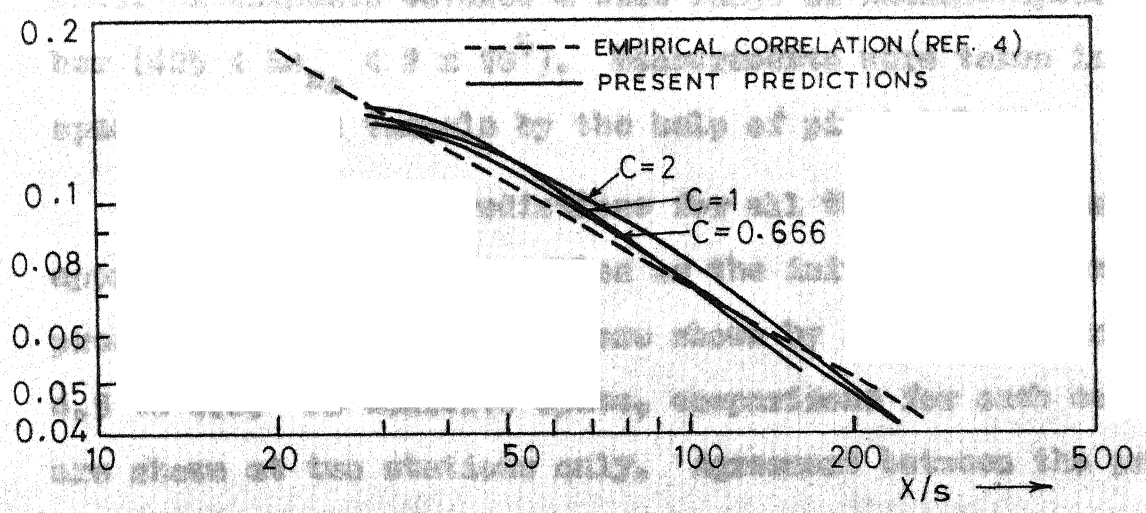

FIG. 4.4 HEAT TRANSFER CHARACTERISTICS.

the jet which is not taken into account by the mixing-length hypothesis.

The Heat-transfer Characteristics:

The heat transfer measurements of Manian et al were presented by a suitable correlation, shown by the dashed line in Fig. 4.4. The solid lines show the present predictions. Once again agreement is found to be fairly good. It is interesting to note that with a diameter to slot height ratio of 0.125, the local Stanton number values for a cylindrical wall jet are as much as 1.8 times that of a plane wall jet under similar conditions.

4.3 Axi-symmetric boundary layer:

There is not much experimental information available for longitudinal flows over circular cylinders. Keshwan (1970) carried out mean-velocity measurements and found that the velocity profiles were not similar. Diameters of the Aluminium cylinders used were 1/16, 1/8, 1/4 and 5.5 inches respectively. Their experiments covered a wide range of radius-Reynolds number ($425 < Re_{r_0} < 2 \times 10^5$). Measurements were taken in low-speed open wind tunnels by the help of pitot tubes.

We have made predictions for all the cases by using appropriate power law profiles as the initial conditions. Our predicted velocity profiles are shown by solid lines in Figs. 4.5 to 4.8. To conserve space, comparisons for each case, are shown at two stations only. Agreement between the predicted

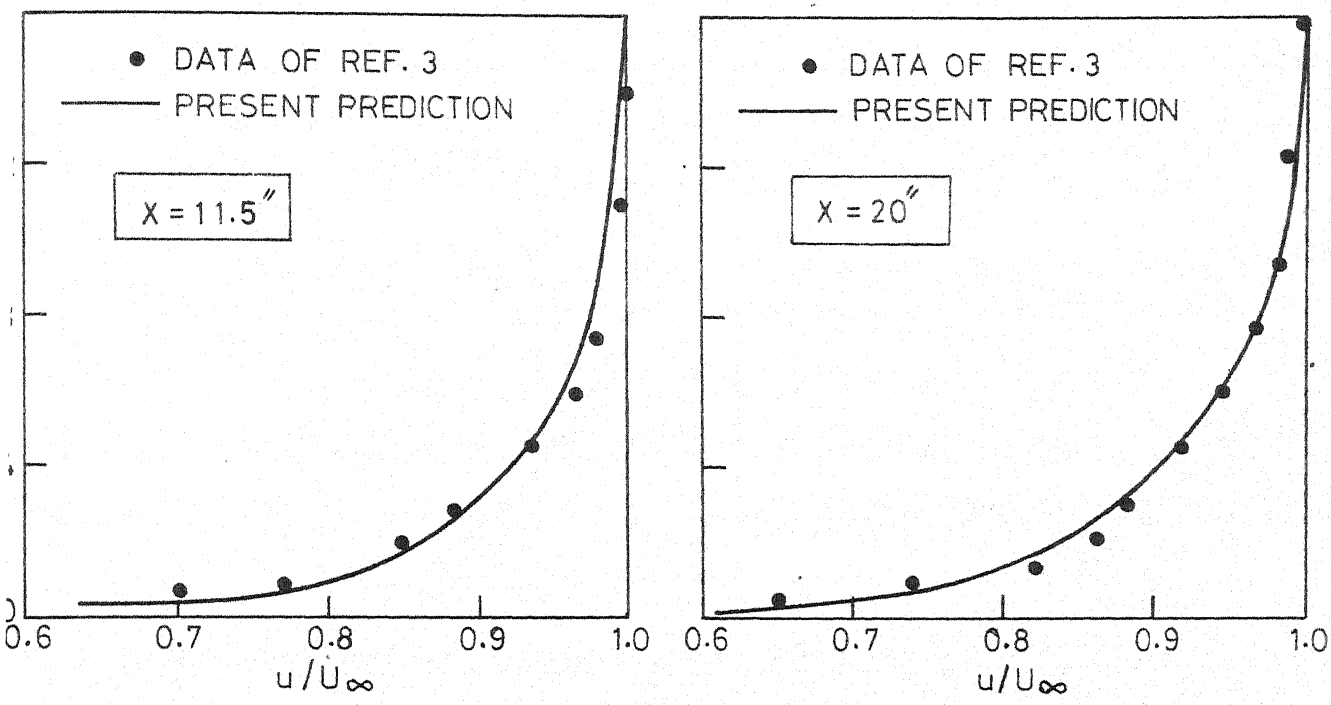

FIG. 4.5 MEAN VELOCITY PROFILES ($2r_o = 1/16''$, $Re_{r_o} = 425$)

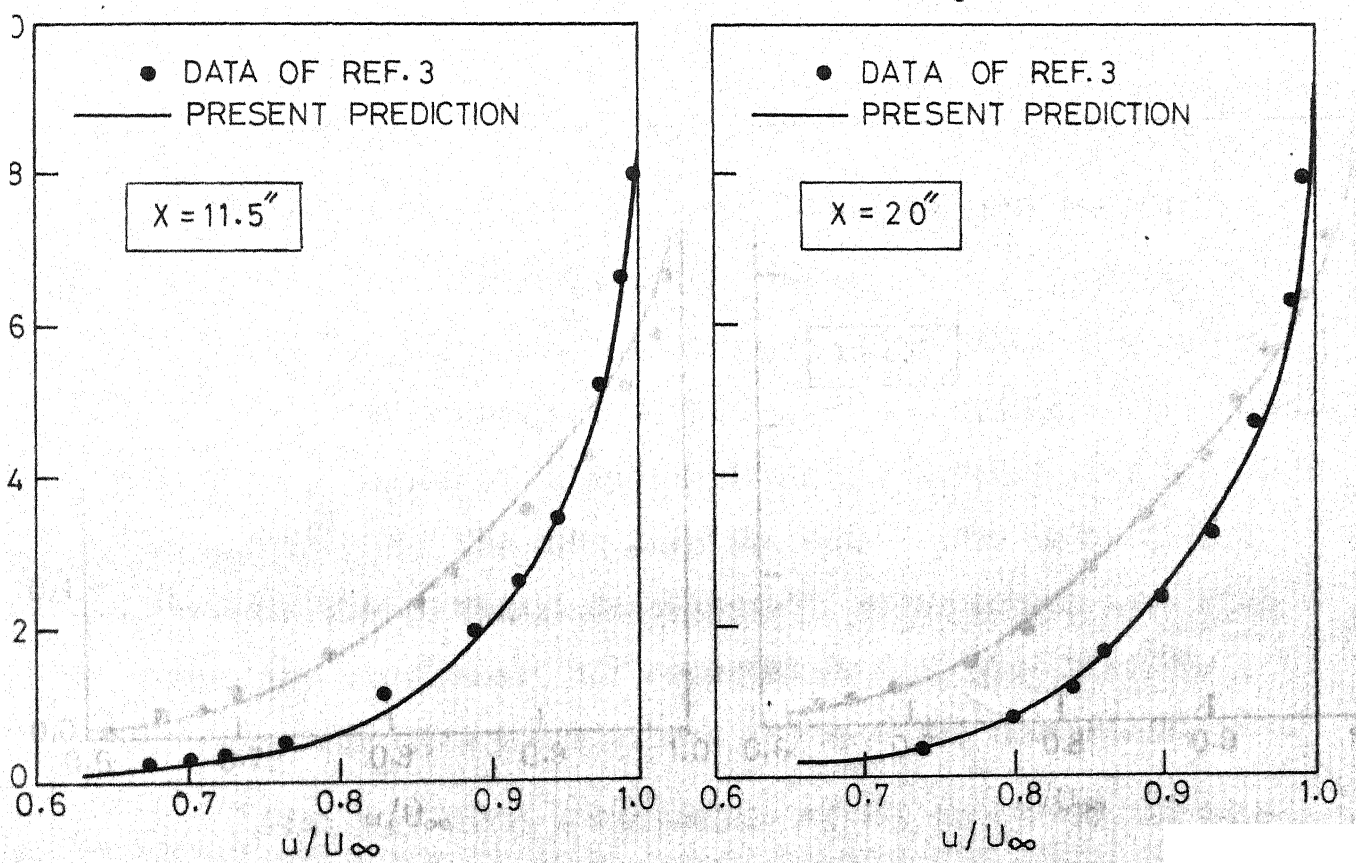

FIG. 4.6 MEAN VELOCITY PROFILES ($2r_o = 1/8''$, $Re_{r_o} = 1640$)

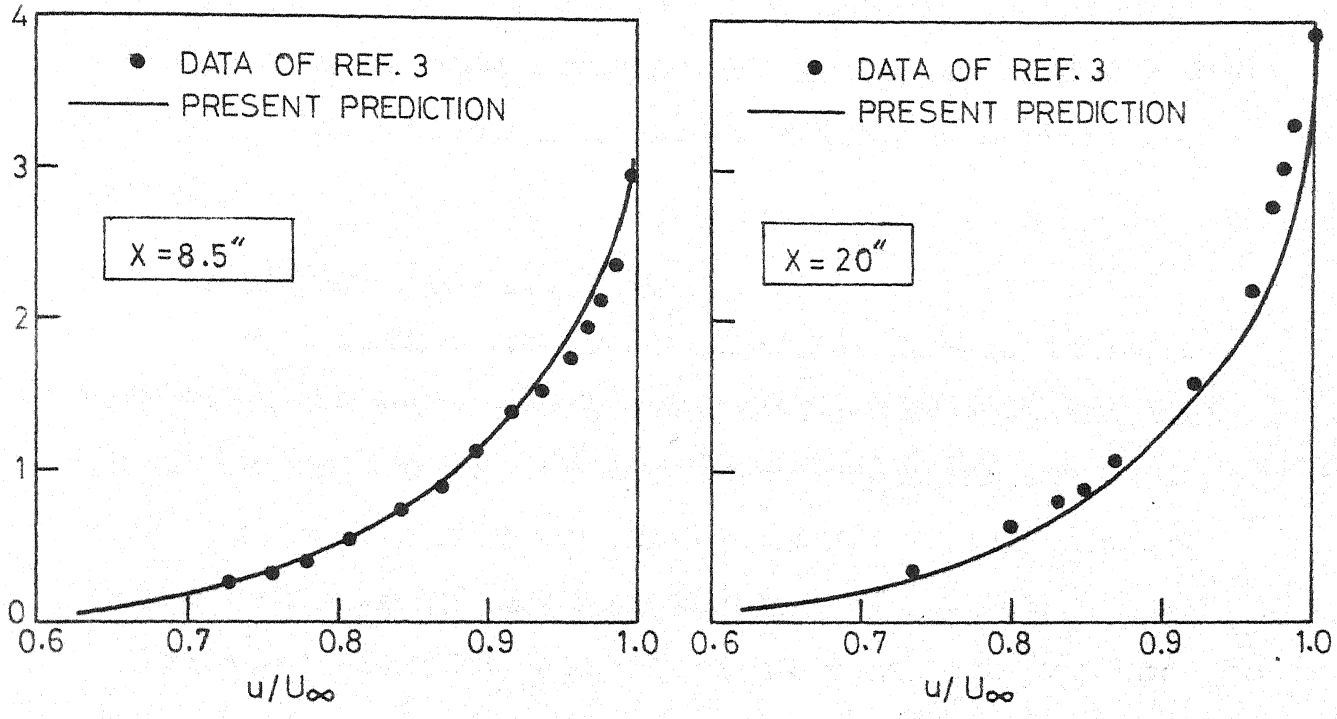

FIG. 4.7 MEAN VELOCITY PROFILES ($2r_o = 1/4''$, $Re_{ro} = 3940$)

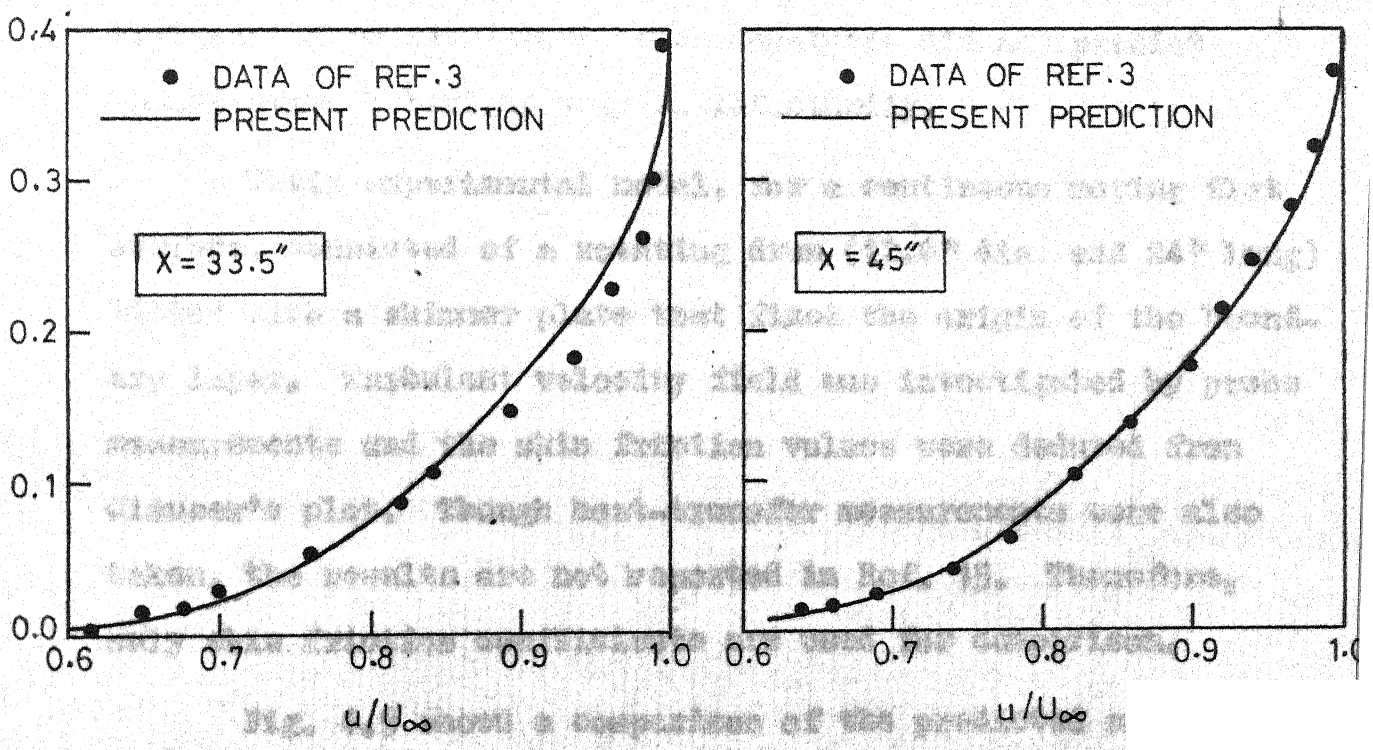

FIG. 4.8 MEAN VELOCITY PROFILES ($2r_o = 5.5''$ $Re_{r_o} = 218500$)

and measured velocity profiles is, in general, satisfactory. Probably more accurate experimental results are needed before making further efforts to improve predictions in such flow situations.

4.4 Continuous Moving Surfaces:

Tsou, Sparrow and Goldstein (1967) have presented an analytical and experimental study of flow and heat-transfer in the boundary layer on a continuous moving surface. They succeeded in obtaining the exact solutions of velocity and temperature fields in laminar-flow situations. They also analysed the turbulent velocity field by applying the concepts of the law of the wall and neglecting the effects of wake-like region at the edge of the boundary layer. However, for turbulent flow situations, their analysis did not predict quantitative behaviour very satisfactorily.

Their experimental model, for a continuous moving flat surface, consisted of a rotating drum (12.6" dia. and 24" long) fitted with a skimmer plate that fixed the origin of the boundary layer. Turbulent velocity field was investigated by probe measurements and the skin friction values were deduced from Clauser's plot. Though heat-transfer measurements were also taken, the results are not reported in Ref. 15. Therefore, only skin friction coefficients are used for comparison.

Fig. 4.9 shows a comparison of the predicted and experimental local skin-friction coefficients. The agreement

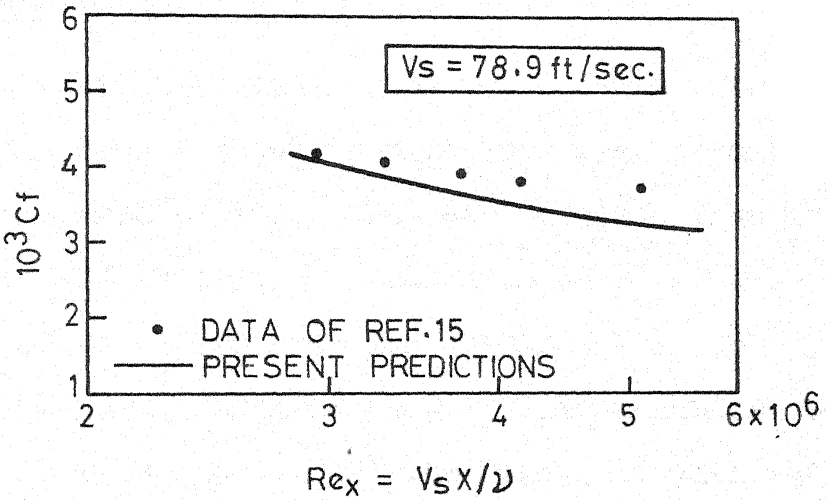

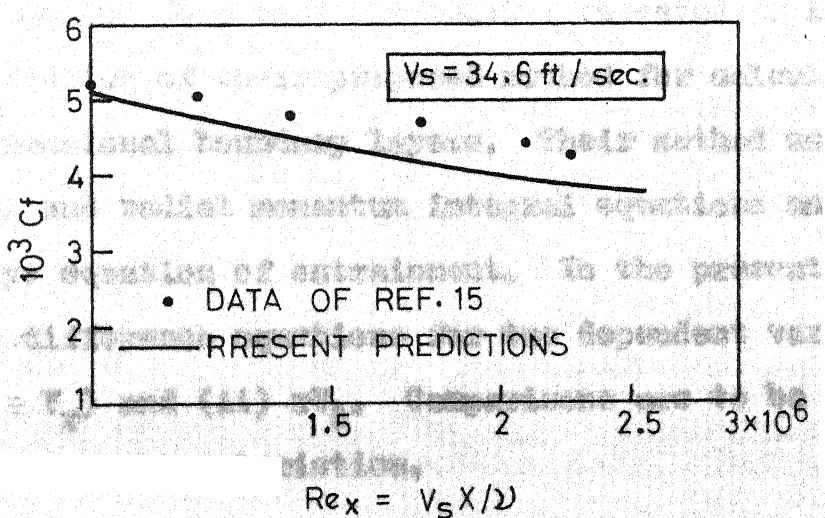

FIG. 4.9 SKIN-FRICTION COEFFICIENT FOR CONTINUOUS MOVING SURFACES

appears reasonably good. It also should be pointed out here that these friction-coefficient values for continuous surface are lower than the corresponding ones for a flat plate.

4.5 Free Rotating Disc:

Detailed measurements of the turbulent boundary layer development over a rotating disc have been recently reported by Cham and Head (1969). They used a steel disc of 3 ft diameter and 1/2" thickness. Measurements were taken at 3 radii for each of the three rotation speeds - 515, 1000 and 1550 r.p.m. The circumferential and radial velocities were deduced by taking cosine and sine of the yaw angle with the total velocity. It was found that turbulent flow regime exists for Reynolds numbers ($\sim r^2/\nu$) higher than 2.85×10^5.

Cham and Head were basically interested in illustrating the application of their proposed method for calculations of three-dimensional boundary layers. Their method used circumferential and radial momentum integral equations and an auxiliarye equation of entrainment. In the present method, we solve difference equations for two dependent variables (i) V_x ($\equiv V_r$) and (ii) rV_θ. Comparisons are to be made for the following characteristics.

(i) circumferential velocity profiles.

(ii) Radial velocity profiles;

(iii) Momentum thickness - Reynolds number, $R\theta_{11}$

(iv) Shape factor, H

(v) Skin friction coefficient, c_f.

The difinitions of the terms involved are:

Radius Reynolds number, $Re_r = \frac{V_o r}{\nu}$ or $\frac{\Omega r^2}{\nu}$

Momentum thickness, $\theta_{11} = \frac{1}{V_o} \int_o^\delta V_\theta (V_o - V_\theta) dy$

Momentum thickness-Reynolds number, $R_{\theta_{11}} = \frac{V_o \theta_{11}}{\nu}$

Displacement thickness, $\delta_1^* = \frac{1}{V_o} \int_o^\delta V_\theta \, dy$

Velocity profile shape factor, $H = \frac{\delta_1^*}{\theta_{11}}$

Tangential skin friction, $Cf_\theta = \frac{\tau_\theta}{1/2 \rho V_o^2}$

Here V_o stands for tangential velocity of moving plate ($V_o \equiv \Omega r$) and the other terms are defined in the same way as in Ref. 2.

We have made predictions of all the above mentioned characteristics for the same three rotational speeds as used by Cham and Head in their experiments. It was evident from our predictions as well as from the experimental results, that a turbulent boundary layer on a rotating disc can be treated as a function of one variable Re_r i.e. Reynolds number based on radius.

Boundary layer growth has been represented by a Reynolds number based on momentum thickness. Fig. 4.11 reveals that the predictions based on two modifications, suggested in Section 2.3, are not very much different from each other and both

the modifications lead to fairly good agreement with the experimental data. Similarly for the velocity shape factor H, it was difficult to differentiate between the results, obtained by the two suggestions. Comparison with the experimental values is shown in Fig. 4.10. For convenience, in the remaining figures we have shown predictions based on Eqn. (2.3-5) only.

Fig. 4.12 reveals that the predicted shear-stress values are not in very good agreement with those of Ref. 2. But the values reported in Ref. 2 may not be exact because these were not experimentally measured, rather they were deduced from Thompson skin-friction relationship and there was no strong justification for its use or validity. Figs. 4.13 and 4.14 show some of the tangential and radial velocity profiles for the angular speed of 1550 r.p.m. Predicted profiles are fairly close to the experimental ones.

4.6 Flow between a rotor and a stator:

Bayley and Owen (1969) carried out experiments to study the flow between rotating and ~~the~~ stationary discs. They measured drag torque and pressure distribution for various mass flow rates, axial gaps and rotation speeds. A 30" dia. disc could be rotated at speeds upto 4500 r.p.m. and results are reported for two axial clearances of 0.45 and 0.12 inches respectively. Radial out flow of air was possible upto 2 lb/sec through a 4" dia pipe. Drag of the rotor was measured by a optical torque-meter.

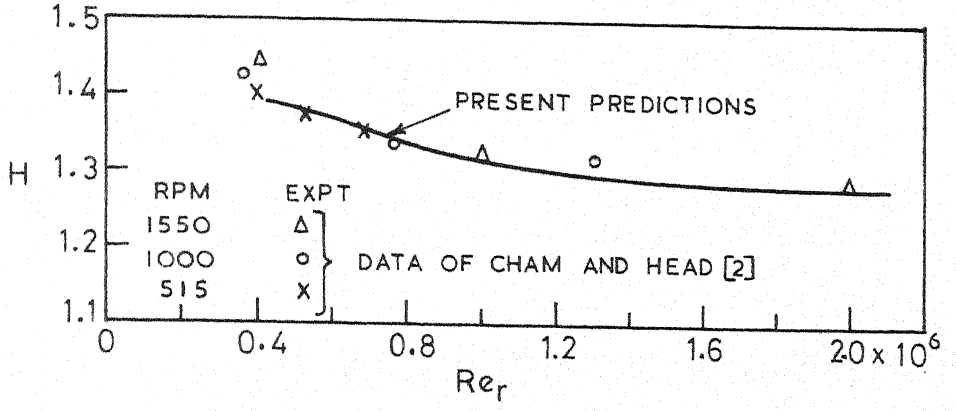

FIG. 4.10 VELOCITY SHAPE FACTOR H

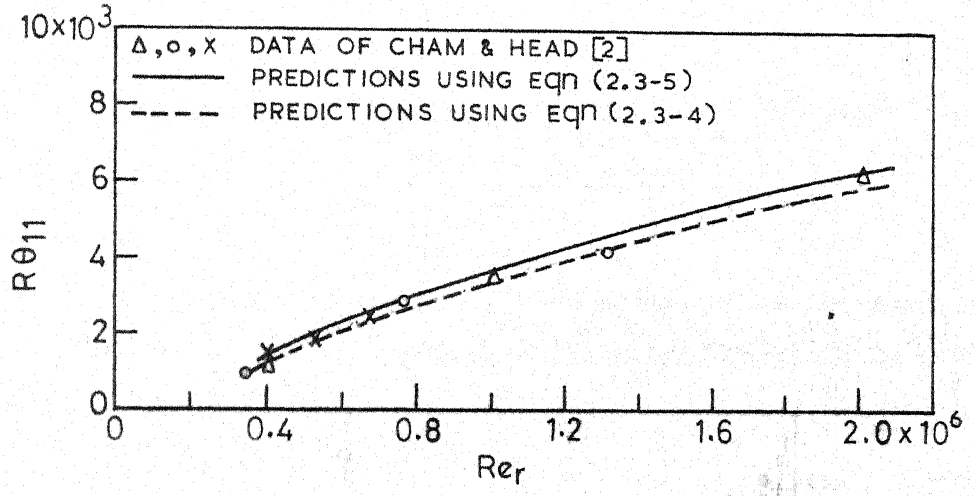

FIG. 4.11 GROWTH OF BOUNDARY LAYER, SHOWN BY REYNOLS NUMBER BASED ON MOMENTUM THICKNESS.

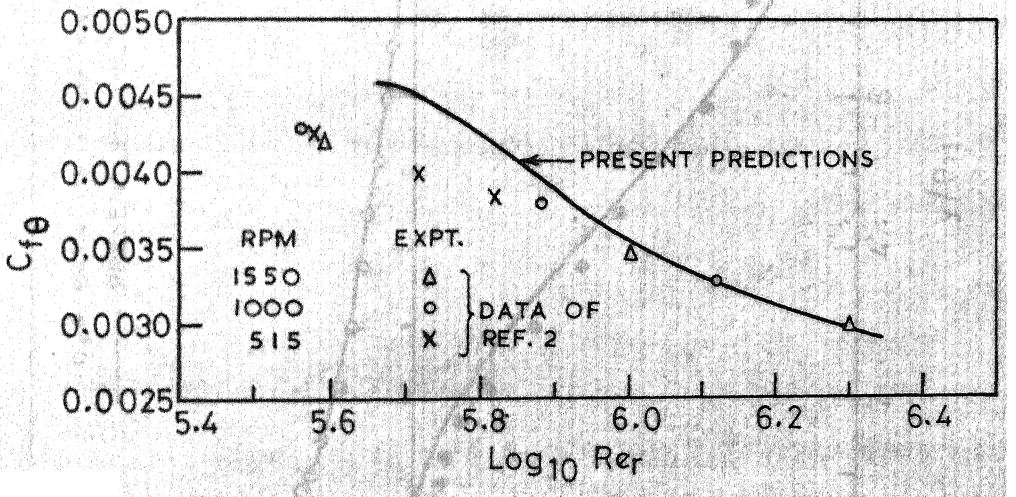

FIG. 4.12 TANGENTIAL SKIN-FRICTION COEFFICIENT $C_{f\theta}$

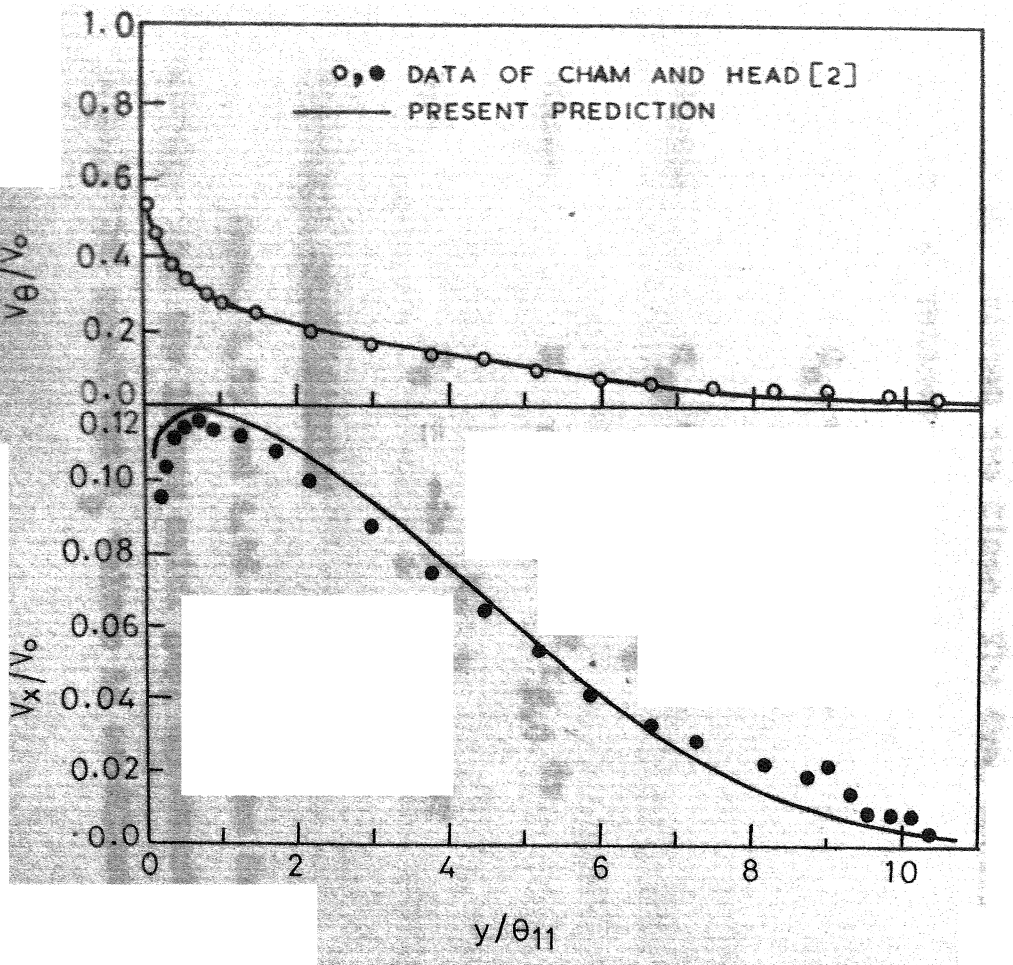

FIG. 4.13 TANGENTIAL AND RADIAL VELOCITY PROFILES AT r = 12 INCHES

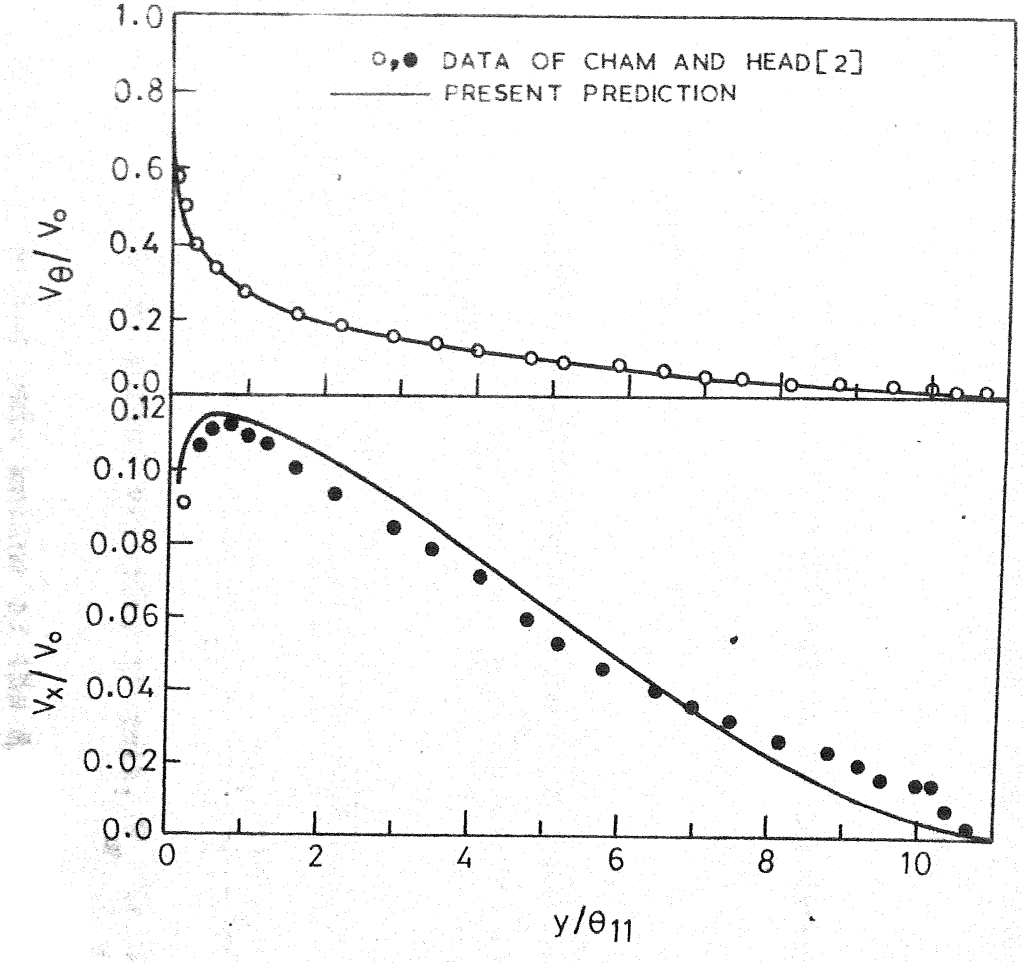

FIG. 4.14 TANGENTIAL AND RADIAL VELOCITY PROFILES AT r = 17 INCHES

Before making comparisons it is necessary to define few terms.

Radius ratio = r/r_o

Radius-Reynolds number, $Re_{r_o} = \frac{\rho \Omega r_o^2}{\mu}$

Gap ratio, $G = S/r_o$

Mass flow coefficient, $C_W = \frac{W}{\mu r_o}$

Pressure coefficient, $C_p = \frac{(p_A - p)\rho r_o^2}{\mu^2}$

Average radial velocity at exit, $V_r = \frac{W}{2\pi r_o S}$

where r_o is the exit radius of the discs and S is the axial clearance between two discs. The drag coefficients have been defined as follows:

Rotor: $C_m = \frac{M}{1/2\ \rho \Omega^2 r_o^5}$

Stator $C_{ms} = \frac{M_s}{1/2\ \rho \Omega^2 r_o^5}$

where $M \equiv -2\pi \int_0^{r_o} r^2 \tau_{\phi,0}\, dr$

and $M_s \equiv -2\pi \int_0^{r_o} r^2 \tau_{\phi,s}\, dr$

<u>Pressure coefficients:</u>

Figs. 4.15 and 4.16 show pressure drop between the two discs. For the larger axial gap, agreement between the experimental and predicted C_p values is excellent over the whole

range of parameters. Fig. 4.15 also includes a curve marked ($\delta A/A$) which reveals the relative area discrepancy.

A remark on area discrepancy in calculation of dp/dx:

Strictly speaking, the external boundary of the flow, decided by our calculations, does not coincide precisely with the stationary disc, for our pressure-gradient procedure permits a discrepancy between the two areas, called as the duct area A_d and the flow area A_f (Section 3.6). To give a better idea of the magnitude of this discrepancy, a non-dimensional quantity ($\delta A/A$) which represents a ratio of discrepancy in area to the duct area, is plotted in Fig. 4.15. It is evident from this figure, as also claimed earlier in Section 3.8, that the area discrepancy has a diminishing tendency. Also it is nowhere greater than 1.5 percent of the duct area. If desired it could be reduced further.

Drag-torque coefficients:

Figs. 4.17 and 4.18 show a comparison between the predicted and experimental drag coefficients for both axial gaps and various mass flow parameters. The departures are nowhere more than 15 percent of the experimental values. It should be noted that for a given mass flow rate and a rotational speed, the integration of tangential stress over the whole disc leads to one value of drag torque. Thus, any error in tangential shear stress will effect the drag torque accumulatively.

Velocity profiles:

Lastly, Fig. 4.19 shows radial and tangential velocity profiles for larger gap and two mass flow rates. Predicted tangential velocity profiles seem to be satisfactory but the radial profiles are not in good agreement with the experimental ones. Velocity measurements were also not very reliable as has been mentioned in Ref. 1. Further it should be noted that the mixing-length model may not correctly reveal the local details of the flow. This defect should not however obscure the fact that the mixing-length hypothesis does at least allow fairly accurate predictions of the gross characteristics.

Now we briefly sum up the main findings of the foregoing study in the next Chapter.

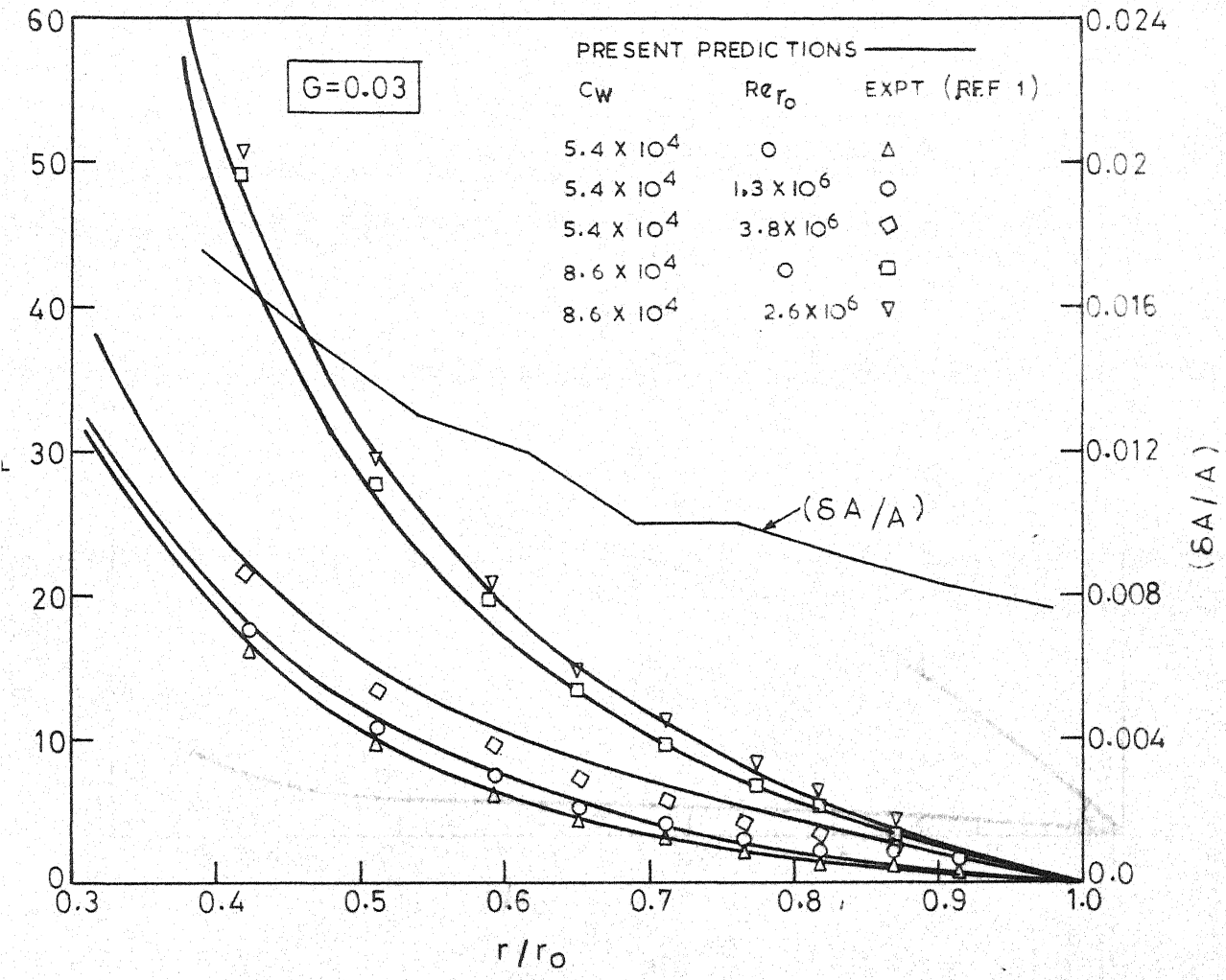

FIG. 4.15 RADIAL PRESSURE DISTRIBUTION G=0.03
(δA/A) RELATIVE AREA DISCREPANCY IN
PRESS CALCULATIONS

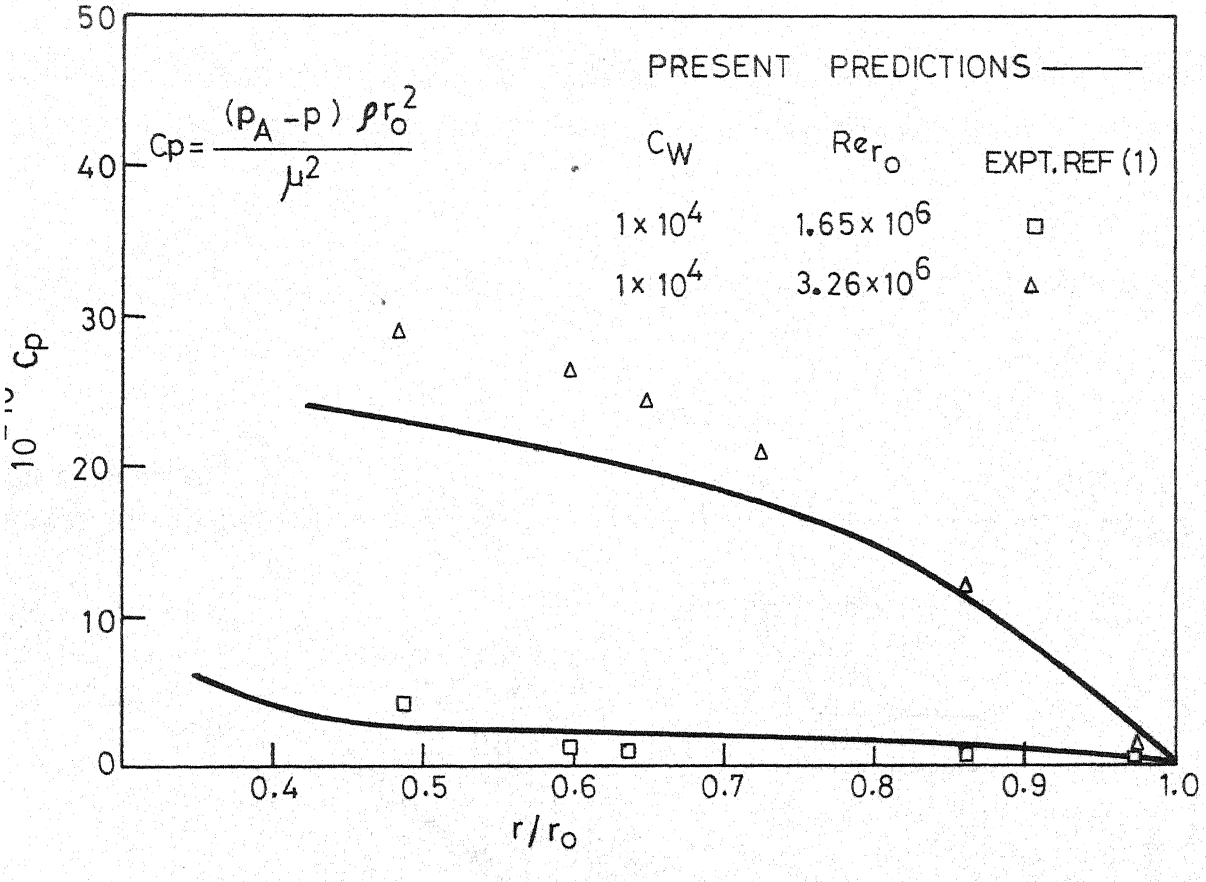

FIG.4.16 RADIAL PRESSURE DISTRIBUTION, G = 0.008

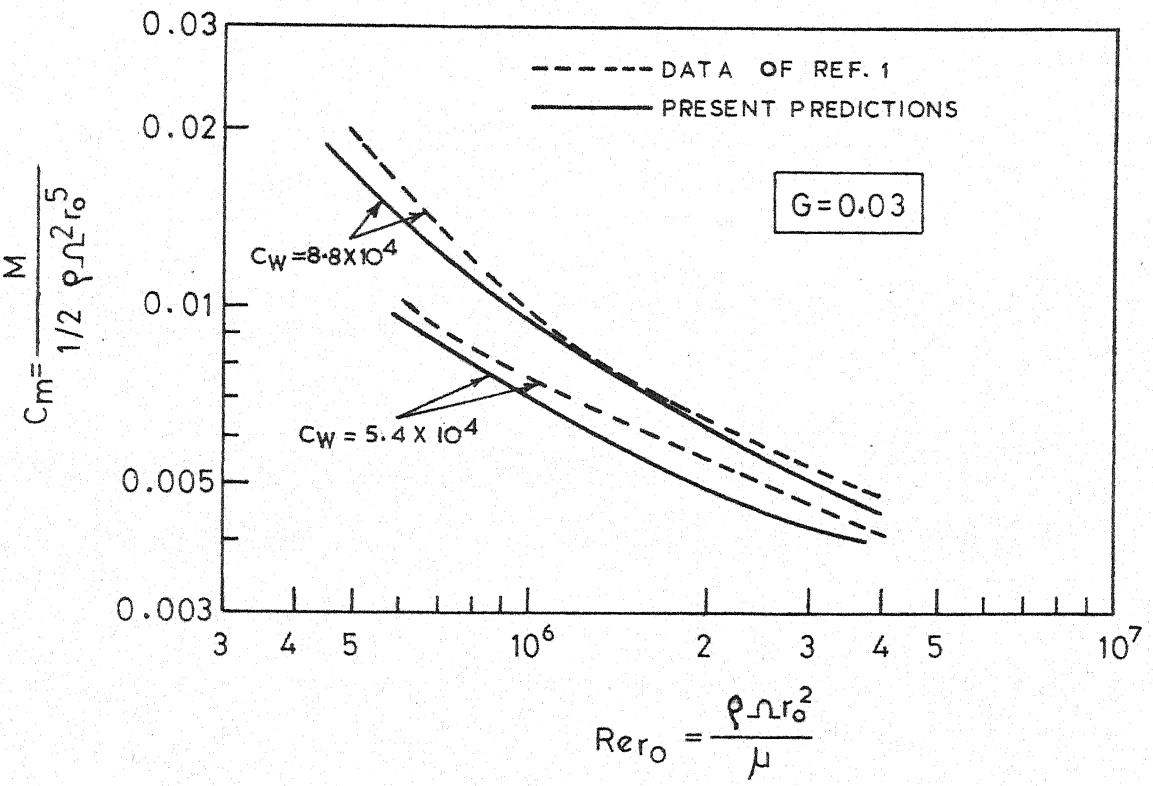

FIG. 4.17 MOMENT COEFFICIENT OF THE ROTOR

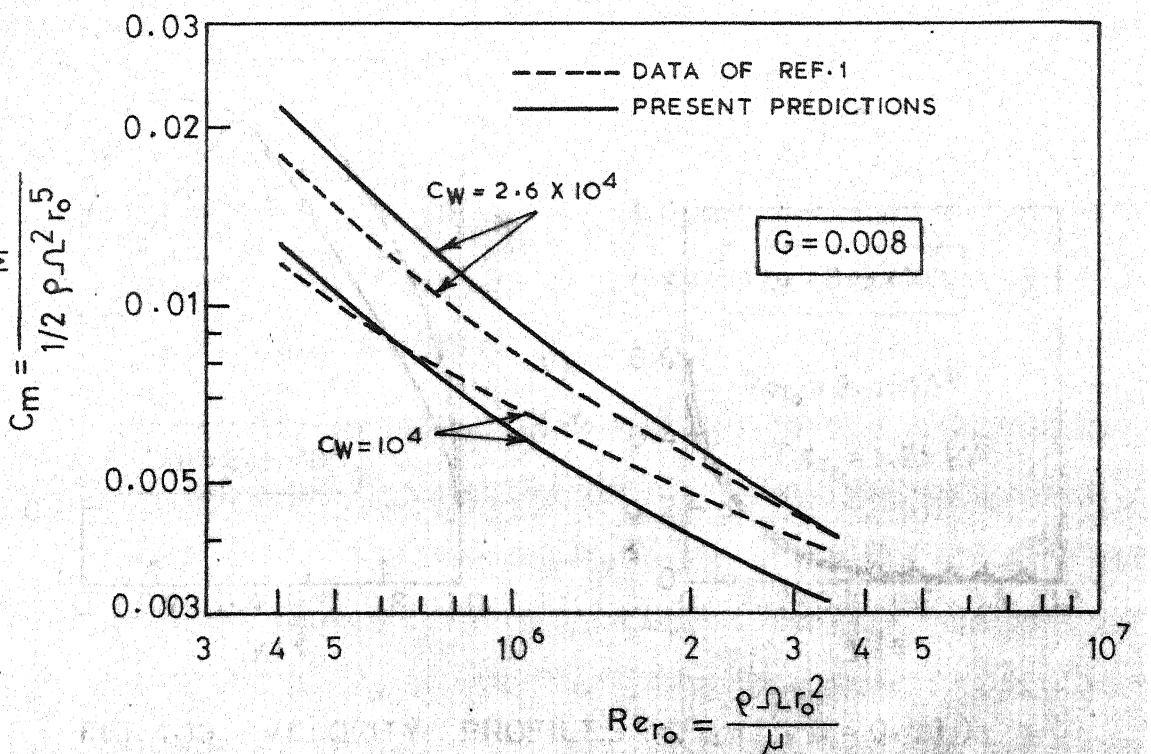

FIG. 4.18 MOMENT COEFFICIENT OF THE ROTOR

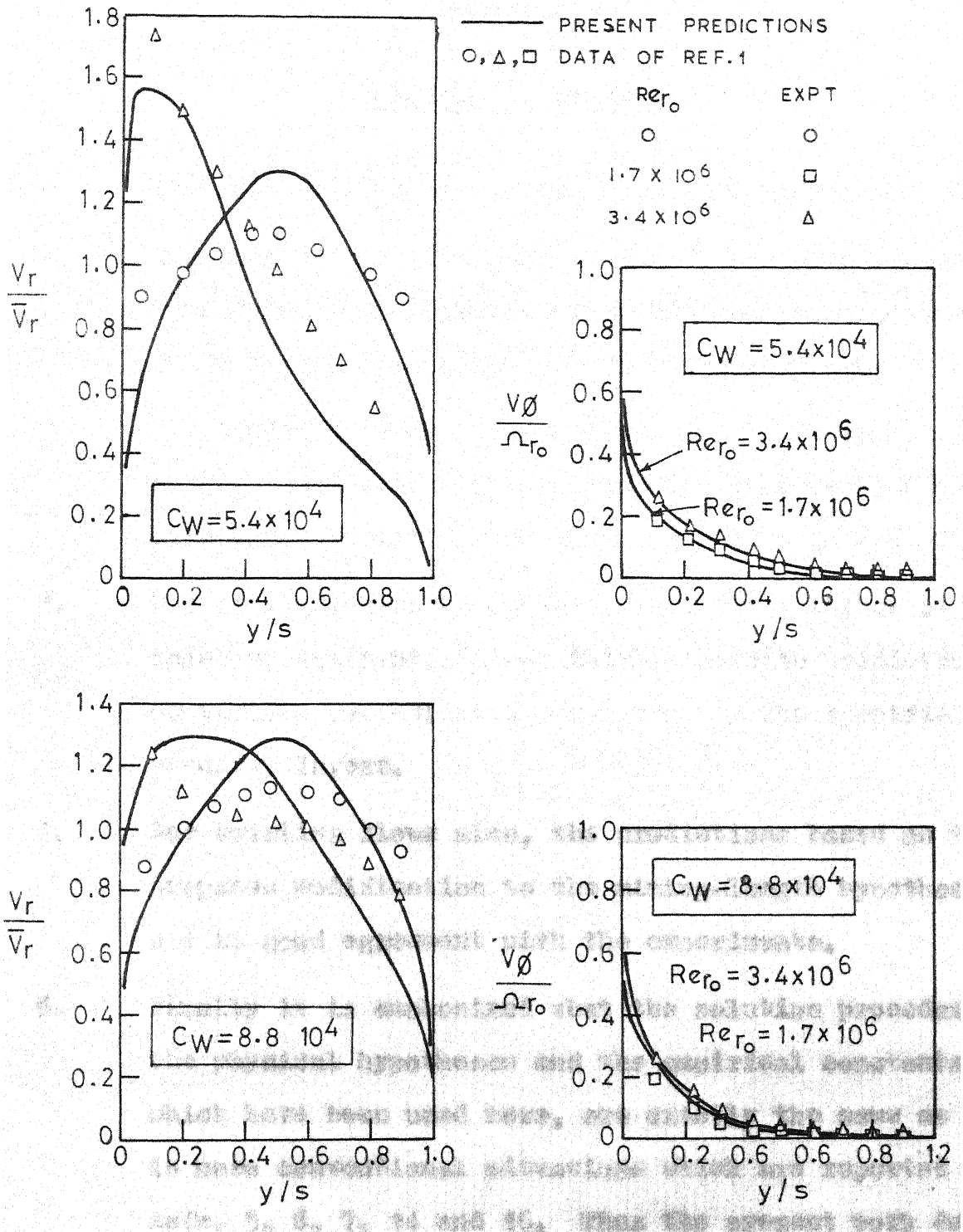

FIG. 4.19 VELOCITY PROFILES ($r/r_o = 1$, $G = 0.03$)

CHAPTER 5

CONCLUDING REMARKS

The main conclusions of the present work are as follows:

1. The calculation procedure of Ref. 7 has been shown to be applicable to a number of flow situations inspite of their unusual geometry or boundary conditions.

2. The important task of prescribing the pressure gradient for confined flows is successfully undertaken with a simple non-iterative scheme as suggested in Ref. 8.

3. The mixing-length hypothesis, with fixed values of the relevant constants, gives fairly accurate predictions of various hydrodynamic properties of the specified boundary layers.

4. For swirling flows also, the predictions based on the proposed modification to the mixing-length hypothesis are in good agreement with the experiments.

5. Finally it is emphasized that the solution procedure, the physical hypotheses and the empirical constants which have been used here, are exactly the same as used in more conventional situations which are reported in Refs. 5, 6, 7, 14 and 16. Thus the present work demonstrates the flexibility and generality of the solution

procedure and also the wider applicability of the particular set of hypotheses and constants.

Suggestions for Future Work:

The over all success of rather simple mixing-length hypothesis encourages the belief that this concept might be very useful in predicting the behaviour of turbulent boundary layers even under more complexed situations.

One could easily extend the present work so as to include various effects like kinetic heating, chemical reaction and variations in fluid properties.

There is ample scope to investigate better hypothesises for swirling flows. However, it would first require enough experimental work.

REFERENCES

1. Bayley, F.J. and Owen, J.M. (1969)
'Flow between a rotating and a stationary disc', Aero Quart., XX, p. 333.

2. Cham, T.S. and Head, M.R. (1969)
'Turbulent boundary layer flow on a rotating disc', J.Fluid. Mech., 37, p. 129.

3. Keshwan, N.R. (1970)
'Axisymmetric incompressible turbulent boundary layer in zero pressure gradient' M.E. Thesis, Department of Aeronautical Engineering, I.I. Sc., Bangalore.

4. Manian, V.S., McDonald, T.W. and Besant, R.W. (1969)
'Heat transfer measurements in cylindrical wall jets', Int. J. Heat Mass Transfer, 12, p. 673.

5. Mahadevan, B. (1969)
'Turbulent boundary layer development in diffusers using finite-difference procedure', M.Tech. Thesis, Dept. of Mechanical Engg., IIT Kanpur.

6. Ng, K.H., Patankar, S.V. and Spalding D.B. (1968)
'The hydrodynamic turbulent boundary layer on a smooth wall, calculated by a finite-difference method', 1968 Symposium on Calculation Method for Turbulent Boundary Layers, Stanford Univereity.

7. Patankar, S.V. and Spalding, D.B. (1967)
'Heat and Mass Transfer in Boundary Layers', Morgan-Grampian press, London, 1967.

8. Second Edition of Ref. 7, to be published by International Text book Co. Ltd., London, 1970.

9. Patankar, S.V. and Spalding, D.B. (1967)
'A finite-difference procedure for solving the equations of the two-dimensional boundary layer', Int. J. Heat Mass Transfer, 10, p. 1389.

10. Sakiadis, B.C. (1961)
'Boundary layer behaviour on continuous solid surfaces: I. Boundary layer equations for two dimensional and axi-symmetrical flow', A.I.Ch. E., J 17, p. 26.

11. Spalding, D.B. (1964)
'A unified theory of friction, heat transfer and mass transfer in the turbulent boundary layer and wall jet', ARC Report 25, 925, MM 3459, HMT 41.

12. Spalding, D.B. (1967)
'Theories of the turbulent boundary layers', Applied Mechanics Review, Vol. 20, 1967, pp. 735.

13. Starr, J.B. and Sparrow, E.M. (1967)
'Experiments on turbulent cylindrical wall jet', J. Fluid. Mech., 29, p. 495.

14. Subramanya, A.R. (1969)
'Effects of surface roughness on hydrodynamic and thermal boundary layers', M. Tech. Thesis, Mech. Engg. Dept., IIT, Kanpur.

15. Tsou, F.K., Sparrow, E.M. and Goldstein, R.J. (1967)
'Flow and heat transfer in the boundary layer on a continuous moving surface', Int. J. Heat Mass Transfer, 10, p. 219.

16. Van Driest, E.R. (1956)
'On turbulent flow near a wall', J. Aeronaut. Sci., 23, 1007.

NOMENCLATURE

C	curvature parameter (rod diameter/slot height)
C_f	skin-friction coefficient
C_m	drag torque coefficient for the rotor
C_{ms}	drag torque coefficient for the stator
C_p	pressure coefficient
C_w	mass flow coefficient
G	gap ratio
H	velocity shape factor
h	specific enthalpy
K	a constant in the mixing length formula
l	mixing length
p	pressure
p_A	atmospheric pressure
q	heat flux in the y direction
r	distance from the axis of symmetry
r_o	radius of a cylinder or exit radius of a disc
R_e	Reynolds number
s	slot height or axial clearance between two discs
S_t	Stanton number
V_x, V_y, V_θ	velocities in x, y and θ directions respectively
V_{max}	maximum velocity
V_s	velocity of the moving surface
V_o	tangential velocity of rotating surfaces

W mass flow rate between two discs

x distance in the streamwise direction

y cross stream distance from the internal boundary

y_1 characteristic length in mixing-length hypothesis

$y_{1/2}$ half value thickness of the wall jet

(i.e. $y = y_{1/2}$ where $V_x = \frac{V_{max}}{2}$

δ boundary layer thickness

δ_1^* displacement thickness

θ_{11} momentum thickness

λ a constant in the mixing-length formula

μ_{eff} effective viscosity

μ molecular viscosity

ρ fluid density

σ_t turbulent Prandtl number

σ_{eff} effective Prandtl number

τ shear stress

ν kinematic viscosity

ψ stream function

ω non-dimensional stream function

Ω angular speed of rotation

ϕ a dependent variable

Subscripts:

D the downstream point on a portion of the grid

d duct

E the external boundary of the layer

f flow

G a free boundary

h pertaining to enthalpy

I the internal boundary of the layer

s conditions at the slot or conditions at the moving surface

U the upstream point on a portion of the grid

Additional symbols used in Appendix:

A stagnation enthalpy

k mean kinetic energy of the fluctuating motion per unit mass

l_1, l_2 the length scales in directions 1 and 2

V_1, V_2, V_θ velocities in directions 1, 2 and θ respectively

X_1, X_2, θ generalised coordinates in directions 1 and 2

β the angle made by direction 1 with the symmetry axis

$_{h,eff}$ effective Prandtl number

$_{k,eff}$ effective Prandtl number for the diffusion of k

APPENDIX

The purpose of this appendix is to give general forms of the equations of Section 2.1 in a very general, axisymmetric coordinate system.

The coordinate system:

Fig. A.1 shows the coordinate system. The coordinate directions 1 and 2 are orthogonal or nearly so. The values of the coordinates are X_1 and X_2, so defined that the element of distance d_s in a plane through the axis of symmetry is given by

$$ds = \sqrt{[(l_1\, dX_1)^2 + (l_2\, dX_2)^2]} \qquad (A-1)$$

The length scales l_1 and l_2 can be defined later. The direction of the constant X_2 lines is so chosen that it is nearly parallel to the local direction of the velocity component in the plane of the diagram. The constant X_2 lines make the angle β with the symmetry axis. The constant X_1 lines are, correspondingly, everywhere almost perpendicular to stream lines.

The equations:

The boundary layer equations in the above mentioned coordinate system will take the following form.

Mass Conservation:

$$\frac{\partial}{\partial X_1}(x l_2 \rho V_1) + \frac{\partial}{\partial X_2}(x l_1 \rho V_2) = 0 \qquad (A-2)$$

or alternatively:

$$\rho V_1 = \frac{1}{r l_2} \frac{\partial \Psi}{\partial X_2}, \quad \rho V_2 = -\frac{1}{r l_1} \frac{\partial \Psi}{\partial X_1} \qquad (A-3)$$

Momentum conservation in direction 1:

$$\frac{\rho V_1}{l_1} \frac{\partial V_1}{\partial X_1} + \frac{\rho V_2}{l_2} \frac{\partial V_1}{\partial X_2} = \frac{1}{r l_1 l_2} \frac{\partial}{\partial X_2} \left(\frac{r l_1}{l_2} \mu_{eff} \frac{\partial V_1}{\partial X_2} \right)$$

$$- \frac{1}{l_1} \frac{\partial p}{\partial X_1} + \rho V_1 V_2 \frac{\partial \beta}{\partial X_1} + \frac{\rho V_\theta^2}{r} \sin \beta \qquad (A-4)$$

Momentum conservation in direction 2:

$$0 = -\frac{1}{l_2} \frac{\partial p}{\partial X_2} - \frac{\rho V_1^2}{l_2} \frac{d\beta}{dX_1} + \frac{\rho V_\theta^2}{r} \cos \beta \qquad (A-5)$$

Momentum conservation in direction θ:

$$\frac{\rho V_1}{l_1} \frac{\partial V_\theta}{\partial X_1} + \frac{\rho V_2}{l_2} \frac{\partial V_\theta}{\partial X_2} = \frac{1}{r l_1 l_2} \frac{\partial}{\partial X_2} \left(\frac{r^2 l_1 \mu_{eff}}{l_2 \sigma_{\theta,eff}} \frac{\partial (V_\theta / r)}{\partial X_2} \right)$$

$$- \frac{\rho V_r V_\theta}{r} \qquad (A-6)$$

Equation for stagnation enthalpy h:

$$\frac{\rho V_1}{l_1} \frac{\partial \tilde{h}}{\partial X_1} + \frac{\rho V_2}{l_2} \frac{\partial \tilde{h}}{\partial X_2} = \frac{1}{r l_1 l_2} \frac{\partial}{\partial X_2} \left[\frac{r l_1}{l_2} \mu_{eff} \times \right.$$

$$\left\{ \frac{1}{\sigma_{h,eff}} \frac{\partial \tilde{h}}{\partial X_2} + \left(\frac{1}{\sigma_{k,eff}} - \frac{1}{\sigma_{h,eff}} \right) \frac{\partial k}{\partial X_2} + \left(1 - \frac{1}{\sigma_{h,eff}} \right) \right.$$

$$\left. \left. \frac{\partial}{\partial X_2} \left(\frac{V_1^2}{2} \right) + \left(\frac{1}{\sigma_{\theta,eff}} - \frac{1}{\sigma_{h,eff}} \right) \frac{\partial}{\partial X_2} \left(\frac{V_\theta^2}{2} \right) - \right. \right.$$

$$\left. \left. \frac{1}{\sigma_{\theta,eff}} \frac{l_2^2}{r l_1} V_\theta^2 \cos \beta \right\} \right] \qquad (A-7)$$

The Eqns. (A-4), (A-6) and (A-7) can be regarded as possessing the common form:

$$\frac{\rho V_1}{l_1}\frac{\partial \phi}{\partial X_1} + \frac{C_2}{l_2}\frac{\partial \phi}{\partial X_2} = \frac{1}{l_1 l_2 r}\frac{\partial}{\partial X_2}\left(\frac{r l_1}{l_2}\frac{\mu_{eff}}{\sigma_{\phi,eff}}\frac{\partial \phi}{\partial X_2}\right) + d \qquad (A\text{-}8)$$

Here ϕ stands for any of the dependent variables e.g. V_1, V_θ or h; and d stands for terms appearing on the right-hand side which do not contain $\partial\phi/\partial X_2$. The other symbols have the significance given in nomenclature.

These equations can be easily cast into any desired coordinate system by making proper choices of the length scales l_1 and l_2. In Ref. 9, l_2 has been so chosen that the equations are directly transformed into the $x \sim \omega$ coordinate system. To get the equations into the same forms as given in Section 2.1 we use a particular form of the above system. The main features of this coordinate system are illustrated in Fig. A-2. The diagram is self-explanatory.

The general coordinates X_1 and X_2 are replaced by x and y respectively, and both the length scales, l_1 and l_2, are taken as unity. This is true only when β does not vary with x, or approximately true if the variation is slow.

The particular form of Eqn. (A-5) will now imply:

$$\frac{\partial p}{\partial y} = -\rho V_x^2 \frac{d\theta}{dx} + \frac{\rho V_\theta^2}{r}\cos\beta \qquad (A\text{-}9)$$

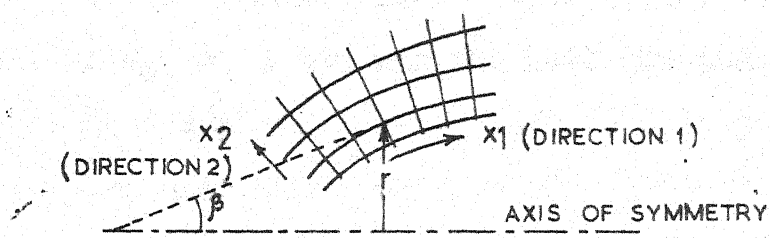

FIG. A-1 THE GENERAL CO-ORDINATE SYSTEM FOR AXI-SYMMETRICAL FLOW.

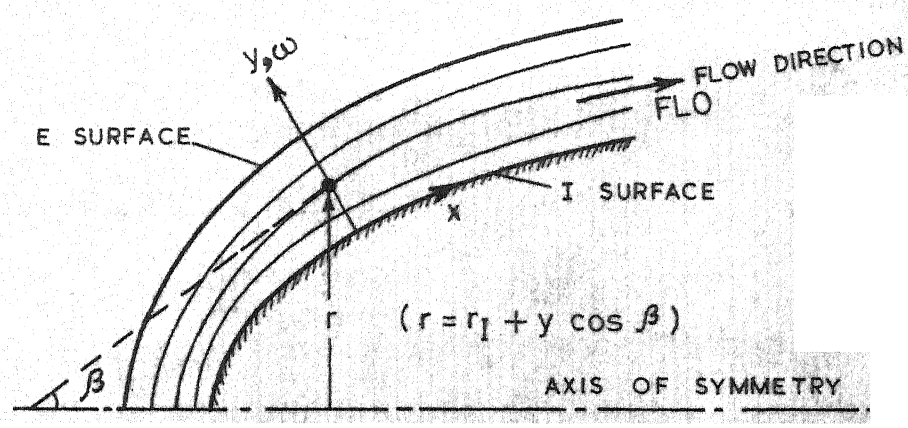

FIG. A-2 THE PARTICULAR CO-ORDINATE SYSTEM

In all our problems $d\beta/dx$ is zero because I surfaces have no curvature in the x direction. Further, for the first three problems $V_\theta = 0$ and for the last two problems though V_θ is not zero, Cos $\beta = 0$ because there β equals 90°. Thus, in the foregoing problems, pressure was taken as uniform across the layer. It should be noted that the calculation-procedure of Ref. 8 is capable of solving problems where pressure varies in y direction also.

Date Due
